

# On the absorption of microwaves by the one-dimensional spin-1/2 Heisenberg-Ising magnet

Michael Brockmann, Frank Göhmann, Michael Karbach, and Andreas Klümper  
*Fachbereich C – Physik, Bergische Universität Wuppertal, 42097 Wuppertal, Germany*

Alexander Weiße  
*Max-Planck-Institut für Mathematik, P.O. Box 7280, 53072 Bonn, Germany*

We analyze the absorption of microwaves by the Heisenberg-Ising chain combining exact calculations, based on the integrability of the model, with numerical calculations. Within linear response theory the absorbed intensity is determined by the imaginary part of the dynamical susceptibility. The moments of the normalized intensity can be used to define the shift of the resonance frequency induced by the interactions and the line width independently of the shape of the spectral line. These moments can be calculated exactly as functions of temperature and strength of an external magnetic field, as long as the field is directed along the symmetry axis of the chain. This allows us to discuss the line width and the resonance shift for a given magnetic field in the full range of possible anisotropy parameters. For the interpretation of these data we need a qualitative knowledge of the line shape which we obtain from fully numerical calculations for finite chains. Exact analytical results on the line shape are out of reach of current theories. From our numerical work we could extract, however, an empirical parameter-free model of the line shape at high temperatures which is extremely accurate over a wide range of anisotropy parameters and is exact at the free fermion point and at the isotropic point. Another prediction of the line shape can be made in the zero-temperature and zero magnetic field limit, where the sufficiently anisotropic model shows strong absorption. For anisotropy parameters in the massive phase we derive the exact two-spinon contribution to the spectral line. From the intensity sum rule it can be estimated that this contribution accounts for more than 80% of the spectral weight if the anisotropy parameter is moderately above its value at the isotropic point.

## I. INTRODUCTION

Short-range antiferromagnetic exchange interactions are the predominant electronic interactions in Mott insulators. They are modeled by the Heisenberg-Ising Hamiltonian

$$H = J \sum_{\langle ij \rangle} (s_i^x s_j^x + s_i^y s_j^y + (1 + \delta) s_i^z s_j^z), \quad (1)$$

where the sum is over nearest-neighbor sites, and  $J$  measures the strength of the exchange interaction. The operators  $s_i^\alpha$  are local spin- $\frac{1}{2}$  operators, and the parameter  $\delta$  takes account of a possible exchange anisotropy and may include the effects of dipolar interactions as well.

A sensitive experimental probe of magnetic interactions in solids is the absorption of microwaves, typically in ESR-experiments. In the simplest experimental setup a circularly polarized wave travels along the direction of a homogeneous magnetic field. The field is slowly changed and one or more absorption lines are observed with increasing field, whose precise location and width depends on the temperature.

For experimentally accessible strengths of the incident microwaves linear response theory<sup>1</sup> provides a satisfactory theoretical frame for the calculation of the absorbed intensity. Then the key quantity to be calculated for a given Hamiltonian is the (imaginary part of) the dynamical susceptibility. It is the Fourier transform of a certain dynamical spin-spin correlation function (see below). Since such a quantity cannot be calculated for an interacting many-body system as the antiferromagnetic Heisenberg-Ising model (1), various kinds of approximations have been tried in the past. Most of these approximations break down, when many-body correlation effects are strong, in particular in one- and two-dimensional systems with strong exchange interactions.

In this work we shall concentrate on the one-dimensional spin- $\frac{1}{2}$  case which is not covered by the more traditional approaches.<sup>1,2</sup> It is relevant for the description of quasi one-dimensional compounds<sup>3,4</sup> with strong exchange interactions. This case has been successfully studied by field theoretical methods<sup>5</sup> which are, however, restricted to small temperatures and to a limited range of magnetic fields. They also seem to have built in certain *a priori* assumptions about the line shapes. In one dimension purely numerical approaches<sup>6,7</sup> are efficient as well. They are unbiased, yet the extrapolation of the data to the thermodynamic limit of large chains may require additional justification and support from analytical calculations.

The aim of the present work is to establish a number of exact results for the microwave absorption of the one-dimensional spin- $\frac{1}{2}$  Heisenberg-Ising magnet, with the homogeneous magnetic field along the magnetic symmetry axis of the chain, and to interpret these results in the light of numerical calculations. In turns the quality and validity of the numerical calculations can be estimated from the analytical results.

Our work is motivated by the recent progress in calculating static short-range correlation functions of the integrable spin- $\frac{1}{2}$  Heisenberg-Ising chain at finite temperatures and magnetic fields. This makes it possible to extend a remarkable result for the resonance shift in one-dimensional antiferromagnetic chains, which was obtained by Maeda et al.<sup>8</sup> and which utilizes the exact nearest-neighbor correlation functions of the isotropic spin- $\frac{1}{2}$  Heisenberg chain. We present an alternative framework for the derivation of the resonance shift which, in the limit of small anisotropy, reproduces the result of Ref. 8. In our approach the anisotropy is treated non-perturbatively. It allows us, moreover, to derive an exact formula for the line width at fixed magnetic field.

We utilize the fact that the absorbed intensity  $I(\omega, h)$  is a

positive function, whose integral over  $\omega$  exists. The field-dependent moments of the corresponding normalized intensity turn out to be static short-range correlation functions which can be calculated directly for the infinite chain. The first moment is the average absorption frequency. In case that there is a single pronounced absorption line it gives a measure for the shift of the resonance compared to the paramagnetic absorption frequency  $\omega = h$  (in the units used in this work). This measure is completely independent of the actual shape of the spectral line. Similarly, the second moment provides a shape-independent measure of the line width. The idea of using moments was introduced by van Vleck<sup>9</sup> even before the linear response theory was created. Here we combine it with the finite-temperature linear response theory. The results of van Vleck are then recovered in the infinite-temperature limit.

Alternatively we may normalize the intensity by its integral over  $h$ . In this case the moments cannot be expressed by finite-range correlation functions. Still, these frequency-dependent moments can be expanded into an infinite series of field-dependent moments<sup>10</sup> which is a useful starting point for approximations such as the high-temperature expansion or an expansion for small anisotropy. Interestingly, the line width defined in terms of the frequency-dependent moments shows a temperature behavior rather different from that determined by the field-dependent moments.

When there is more than a single resonance, the interpretation of the moments is less intuitive. In case of two peaks, for instance, the first moment would be something like the average location of the two peaks. For this reason it is desirable to have some knowledge about the full absorption spectrum ('the line shape'). Hence, we complemented our exact calculation of the moments with numerical calculations of the dynamical susceptibility on finite lattices up to 32 sites. The combination of both, the exact calculation of the moments and the numerics, allows us to propose a model for the line shape in the high-temperature limit which has no free parameters. The actual parameters of the corresponding distribution function (a normal-inverse Gaussian) are determined from the first four exactly calculated moments.

An unbiased but approximate calculation of the line shape is possible in the massive ground state phase of the model at vanishing magnetic field. For an isotropic system there is no absorption without an external field. For sufficiently high anisotropy, however, the absorption becomes large. In the massive phase the matrix elements of the local spin operators between the ground states and excited states ('form factors') are exactly known<sup>11</sup> and generally non-vanishing in the thermodynamic limit. They are classified as  $2n$ -spinon contributions according to the (even) number of elementary excitations involved. Here we calculate the two-spinon contribution to the absorbed intensity exactly. From the intensity sum rule we infer that for anisotropies moderately above the isotropic point the two-spin contribution is dominant and amounts to more than 80% of the absorbed intensity. For growing anisotropy it rapidly approaches 100%. But as opposed to the situation with the dynamic structure factor for which the relative contribution of the two-spinon excitation is still dominant in the isotropic limit,<sup>12-14</sup> it drops off rapidly for the dynamical susceptibility.

## II. THE METHOD OF MOMENTS

For any spin system with Hamiltonian  $H$  linear response theory relates the intensity absorbed from a circularly polarized electro-magnetic wave, whose wave length is large compared to the distance between the spins, to the (imaginary part of the) dynamical susceptibility<sup>1</sup>

$$\chi''_{+-}(\omega, h) = \frac{1}{2L} \int_{-\infty}^{\infty} dt e^{i\omega t} \langle [S^+(t), S^-] \rangle_T. \quad (2)$$

Here  $S^\pm = S^x \pm iS^y$ , and the  $S^\alpha = \sum_{j=1}^L s_j^\alpha$ ,  $\alpha = x, y, z$ , are the components of the total spin.  $L$  is the number of lattice sites,  $\langle \cdot \rangle_T$  stands for the canonical average at temperature  $T$  calculated by means of the statistical operator  $\rho = e^{-(H-hS^z)/T} / \text{tr}\{e^{-(H-hS^z)/T}\}$ . Through this average the dynamical susceptibility depends on  $T$  and on an external homogeneous magnetic field  $h$  which is usually applied in ESR experiments. The time evolution of  $S^+$  in (2) must be calculated with  $H - hS^z$ . The absorbed intensity per spin, normalized by the intensity of the incident wave and averaged over a half-period  $\pi/\omega$  of the microwave field, is

$$I(\omega, h) = \frac{\omega}{2} \chi''_{+-}(\omega, h). \quad (3)$$

In order to keep this paper self-contained we included a derivation of (2) and of (3) in App. A.

In this work we shall exclusively concentrate on the one-dimensional version of the Heisenberg-Ising (or XXZ) Hamiltonian (1). This Hamiltonian is in the class of integrable Hamiltonians, but so far this does not mean that dynamical correlation function such as the expectation value  $\langle [S^+(t), S^-] \rangle_T$  in (2) could be calculated analytically. We are only aware of three very special cases where this is possible. These are the 'free Fermion case'  $\delta = -1$  at  $T \rightarrow \infty$ , the isotropic limit  $\delta \rightarrow 0$  and the Ising limit  $\delta \rightarrow \infty$ . We shall discuss these cases below. In the general case so far only the short time behavior of  $\langle [S^+(t), S^-] \rangle_{T \rightarrow \infty}$  can be accessed by directly calculating the commutators involved in the time evolution up to a certain power. We generated this series up to the order  $t^{38}$  (cf. App. C). Still, the results for the short-time behavior alone are not helpful for calculating the right hand side of (2).

Interestingly enough, as we have shown,<sup>10</sup> some more elementary spectral characteristics, such as the position of the resonance or the line width, are easier to calculate. They may be expressed in terms of certain static correlation functions that determine the moments of a normalized intensity function in one variable. Since  $I(\omega, h)$  is a function of the frequency  $\omega$  and of the magnetic field  $h$  we may normalize it by dividing either by the integral over  $\omega$  or by the integral over  $h$ .

In the first case we interpret the resulting normalized function as a distribution function of frequencies which depends parametrically on the magnetic field. Then its moments  $m_n$  are field dependent. This corresponds to an experimental situation where the field is kept fixed and the frequency is varied. We shall see that, from a theoretical perspective, this case is comparatively simple, since the moments depend only on static correlation functions of finite range. The lowest moments

which determine the position of the resonance and its width can be expressed by correlation functions ranging over up to four lattice sites, which can be calculated exactly.<sup>15,16</sup>

In the second case, when the intensity is normalized as a function of the magnetic field, the corresponding moments  $M_n$  depend on the frequency. This corresponds to the standard ESR setup in which the magnetic field is slowly swept at fixed frequency. As we shall see below this case is more sophisticated for a theoretical analysis, since static correlation functions for arbitrary distances are already involved in the calculation of the lowest moments. Still, the  $M_n$  can be expanded into an infinite series in terms of the moments  $m_n$  and their derivatives, which may serve as a starting point for systematic approximations.

### A. Field-dependent moments

We temporarily assume that our chain is large but finite. Then the spectrum is bounded and the integrals

$$I_n = \int_{-\infty}^{\infty} d\omega \omega^n I(\omega, h) \quad (4)$$

exist for all non-negative integers  $n$ . Since  $I(\omega, h)$  is non-negative everywhere and since  $I_0 > 0$ , we may interpret  $I(\omega, h)/I_0$  as a probability distribution with moments  $I_n$ . As we shall see, in our case it is convenient to express the  $I_n$  in terms of another closely related sequence of integrals

$$m_n(T, h) = J^{-n} \int_{-\infty}^{\infty} \frac{d\omega}{2\pi} (\omega - h)^n \chi''_{+-}(\omega, h) \quad (5)$$

which, by slight abuse of language, we shall call (shifted) moments as well. The existence of the integrals is obvious for every finite chain.

Now by definition the shift of the resonance for fixed  $h$  is the deviation of the average frequency from the paramagnetic resonance at  $\omega = h$ ,

$$\delta\omega = \frac{I_1}{I_0} - h = J \frac{Jm_2 + hm_1}{Jm_1 + hm_0}. \quad (6)$$

A measure for the line width is the mean square deviation from the average frequency

$$\Delta\omega^2 = \frac{I_2}{I_0} - \frac{I_1^2}{I_0^2} = J^2 \frac{Jm_3 + hm_2}{Jm_1 + hm_0} - \delta\omega^2. \quad (7)$$

We see that, in order to calculate the resonance shift and the line width, we need to know the first four shifted moments  $m_0, m_1, m_2, m_3$  of the dynamic susceptibility  $\chi''_{+-}$ .

In the following we shall employ the notation  $\text{ad}_X \cdot = [X, \cdot]$  for the adjoint action of an operator  $X$ . Then  $S^+(t) = e^{-iht} e^{it \text{ad}_H} S^+$ , since  $[H, S^+] = 0$  and  $[S^z, S^+] = S^+$ , and it follows with (2) and (5) that

$$m_n = \frac{1}{2L} \langle [S^+, \text{ad}_{H/J}^n S^-] \rangle_T. \quad (8)$$

The latter formula shows that the moments  $m_n$  are static correlation functions whose complexity grows with growing  $n$ .

The first few of them can be easily calculated. In particular,

$$m_0 = \frac{1}{2L} \langle [S^+, S^-] \rangle_T = \frac{1}{L} \langle S^z \rangle_T \quad (9)$$

which is the magnetization per lattice site. For the subsequent moments, which do not have such an immediate and simple interpretation, we obtain

$$m_1 = \delta \langle s_1^+ s_2^- - 2s_1^z s_2^z \rangle_T, \quad (10a)$$

$$m_2 = \frac{1}{2} \delta^2 \langle s_1^z + 4s_1^z s_2^z s_3^z - 4s_1^z s_2^+ s_3^- \rangle_T, \quad (10b)$$

$$m_3 = \frac{1}{4} \delta^2 \langle 2s_1^+ s_2^+ s_3^- s_4^- + 4s_1^+ s_2^- s_3^+ s_4^- - 2s_1^+ s_2^- s_3^- s_4^+ \\ - 8s_1^z s_2^z s_3^z s_4^- - 4s_1^z s_2^+ s_3^z s_4^- + 8s_1^z s_2^+ s_3^- s_4^+ - 4s_1^+ s_2^- \\ - s_1^+ s_3^- + 8s_1^z s_2^z s_3^z s_4^z + 2s_1^z s_3^z - 4s_1^z s_2^z \\ + \delta(8s_1^z s_2^+ s_3^- s_4^z + 2s_1^+ s_2^- - 8s_1^z s_2^z) \rangle_T. \quad (10c)$$

These moments are certain combinations of static short-range correlation functions which implies, in particular, that they all exist in the thermodynamic limit  $L \rightarrow \infty$ . Hence, we may relax our restriction that we are dealing with a finite chain at this point. An interesting conclusion which can be drawn from the existence of the moments is that the field-dependent line shape cannot be Lorentzian, as is sometimes assumed in the literature, since the second moment of a Lorentzian does not exist. In fact, in our numerical data for finite chains we see an exponential decay away from the resonance (see below). Note that for finite magnetic field  $m_0$  is of order 1,  $m_1$  is of order  $\delta$ ,  $m_2$  is of order  $\delta^2$ , but all higher moments are of order  $\delta^2$  as well. This is clear from (8) and will be relevant below.

The formulae (10) are appealing from a theoretical perspective, since, due to recent progress in the theory of integrable systems, static short-range correlation functions of the Heisenberg-Ising chain can be calculated exactly. It has been shown that all static correlation functions of the one-dimensional Heisenberg-Ising model are polynomials in the derivatives of three functions<sup>17</sup>  $\varphi$ ,  $\omega$ , and  $\omega'$  which, as is common in integrable models, can be expressed in terms of the solutions of certain numerically well behaved linear and non-linear integral equations.<sup>18</sup> We provide the definition of these functions in the critical case ( $-1 < \delta < 0$ ) in App. D. For the massive case ( $\delta > 0$ ) the definitions are similar and can be found in Ref. 16.

Although, in principle, all static correlation functions of the Heisenberg-Ising chain in the thermodynamic limit are known exactly, their explicit calculation works out only at short distances. At larger distances the amount of computer algebra involved in the calculations grows excessively. In Refs. 19, 15, and 16 we obtained all correlation functions ranging over at most four lattice sites. This is just enough to calculate the moments  $m_0, m_1, m_2, m_3$ . For the simpler case of the isotropic model in vanishing magnetic field we obtained the correlation functions ranging over up to seven lattice sites.<sup>20</sup>

When considering the Heisenberg-Ising Hamiltonian as an integrable model it is customary to parameterize all functions by a deformation parameter  $q$  in terms of which the anisotropy is  $\delta = (q - 1)^2/2q$ . Employing the shorthand

notations  $\varphi_{(n)} = \partial_x^n \varphi(x)|_{x=0}$ ,  $f_{(m,n)} = \partial_x^m \partial_y^n f(x,y)|_{x=y=0}$ , for  $f = \omega, \omega'$ , we obtain<sup>10</sup>

$$\begin{aligned}
m_0 &= -\frac{1}{2} \varphi_{(0)}, \\
m_1 &= \frac{(q-1)^2(q^2+4q+1)\omega'_{(0,1)} - (q^3-1)\omega_{(0,0)}}{16q^2} - \frac{(q^3-1)\omega_{(0,0)}}{4q(q+1)}, \\
m_2 &= \frac{(q-1)^2}{256q^4} [4q(q+1)(q^3-1)(\omega_{(0,2)}\varphi_{(0)} - 2\omega_{(1,1)}\varphi_{(0)} - \omega_{(0,0)}\varphi_{(2)}) \\
&\quad + (q^2-1)^2(q^2+4q+1)(\omega'_{(1,2)}\varphi_{(0)} + \omega'_{(0,1)}\varphi_{(2)}) - 16q^2(q-1)^2\varphi_{(0)}], \\
m_3 &= \frac{(q-1)^4}{98304q^8(q^4-1)(q^6-1)} [16q^2(q^2-1)^3(q^4-1)(q^6-1)(q^2+4q+1)(\omega_{(0,2)}\omega'_{(0,1)} + \omega_{(0,0)}\omega'_{(1,2)}) \\
&\quad + 64q^2(q^2-1)^4(2q^{10}-q^9+4q^8-4q^7-12q^6-14q^5-12q^4-4q^3+4q^2-q+2)\omega_{(0,0)}\omega_{(1,1)} \\
&\quad - 16q^2(q^2-1)^2(q^4-1)(q^6-1)(3q^4+14q^2+3)\omega'_{(0,3)} + 8q^2(q^2-1)(q^4-1)^2(q^6-1)(q+1)^2(8\omega'_{(1,2)} - \omega'_{(2,3)}) \\
&\quad + 192q^4(q^2-1)^2(q^4-1)(q^6+18q^4+8q^3+18q^2+1)\omega_{(0,2)} \\
&\quad + 64q^2(q^2-1)^2(q^4-1)(q+1)^2(2q^8-5q^7+26q^6-49q^5+28q^4-49q^3+26q^2-5q+2)\omega_{(1,1)} \\
&\quad - 16q^2(q^2-1)^2(q^4-1)(q+1)^2(q^8-q^7+q^6+q^5+2q^4+q^3+q^2-q+1)(2\omega_{(1,3)} - 3\omega_{(2,2)}) \\
&\quad + 64q^2(q^4-1)(q^6-1)(3q^8+2q^6+24q^5-130q^4+24q^3+2q^2+3)\omega'_{(0,1)} \\
&\quad + (q^4-1)(q^6-1)(q+1)^2(q^{10}-2q^9+25q^8+16q^7+118q^6+164q^5 \\
&\quad \quad + 118q^4+16q^3+25q^2-2q+1)(\omega'_{(0,3)}\omega'_{(1,2)} + \omega'_{(0,1)}\omega'_{(2,3)}) \\
&\quad - 1536q^5(q^4-1)(4q^8-9q^7-2q^6-6q^5+8q^4-6q^3-2q^2-9q+4)\omega_{(0,0)} \\
&\quad + 4q^2(q^6-1)(q+1)^2(q^2+1)(5q^8-2q^7+32q^6+50q^5+70q^4+50q^3+32q^2-2q+5) \\
&\quad \quad (2\omega_{(1,3)}\omega'_{(0,1)} - 3\omega_{(2,2)}\omega'_{(0,1)} + \omega_{(0,2)}\omega'_{(0,3)} - 2\omega_{(1,1)}\omega'_{(0,3)} - 3\omega_{(0,2)}\omega'_{(1,2)} - \omega_{(0,0)}\omega'_{(2,3)}) \\
&\quad - 16q^2(q+1)^2(q^{16}-q^{15}+8q^{14}+9q^{13}+47q^{12}+45q^{11}+96q^{10}+91q^9+128q^8+91q^7+96q^6 \\
&\quad \quad + 45q^5+47q^4+9q^3+8q^2-q+1)(3\omega_{(0,2)}^2 - 6\omega_{(1,1)}\omega_{(0,2)} + 2\omega_{(0,0)}\omega_{(1,3)} - 3\omega_{(0,0)}\omega_{(2,2)})]. \tag{11}
\end{aligned}$$

These are the moments in the thermodynamic limit. We can calculate them with high numerical accuracy over the whole range of the phase diagram, for all temperatures and magnetic fields as well as for arbitrary anisotropy  $\delta$ . In Figs. 1-3 we show two examples not too far away from the isotropic point, namely  $\delta = -0.1$  in the critical phase and  $\delta = 0.25$  in the massive phase. Values not too far away from the isotropic point are most relevant for real materials. In both cases we observe an increase of the resonance shift  $\delta\omega$  and a broadening of the spectral lines, measured as an increase of  $\Delta\omega$ , for decreasing temperatures.

This is interesting as it seems to contradict experimental results<sup>4</sup> which claim a narrowing. This discrepancy is due to the different measures for the line width here and in the experimental literature. The mean square deviation used in Figs. 1-3 is a customary measure for the width of wave functions in quantum mechanics. For Gaussians it is of the order of magnitude of an intuitive line width drawn by eye, but for distributions which have long and shallow tails this is no longer the case. Hence,  $\Delta\omega$  may strongly deviate from a typical measure of the line width used in the interpretation of experimental data as

e.g. the distance between the inflection points right and left to the maximum of the intensity ('peak-to-peak width'). This discrepancy was already noted by van Vleck.<sup>9</sup> One advantage of the mean square deviation from the resonance frequency as a measure of the line width is that it is defined independently of the line shape. In principle it should be no problem to extract it from experimental data. Yet, we expect that in cases, where the contributions from the tails of the spectral line are important, a problem might be to resolve these tails from the 'background'.

The difference between different measures of the line width becomes rather clear from our numerical analysis below (compare also Ref. 7). For high temperatures, where we could extract a model for the line width from our numerical data, the 'peak-to-peak width' is much smaller than  $\Delta\omega$ . This can be attributed to the shallow tails of the absorbed intensity. In experiments these tails may be misinterpreted as stemming from couplings of the spin chain to other degrees of freedom and may lead to an overestimation of the background. On the other hand, tails are expected to have less influence on the resonance shift. As long as they are not too asymmetric the

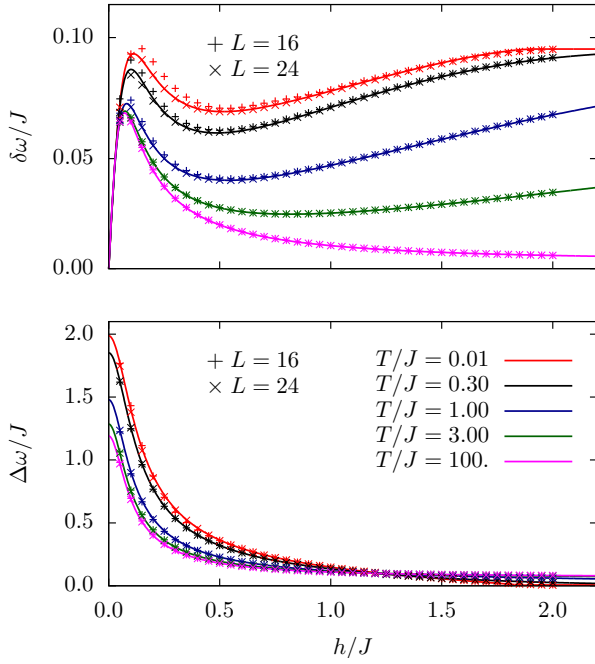


FIG. 1. Resonance shift  $\delta\omega/J$  and line width  $\Delta\omega/J$  in the critical regime at  $\delta = -0.1$  as function of the magnetic field. Crosses from fully numerical calculation for finite chain Hamiltonians of 16 and 24 sites.

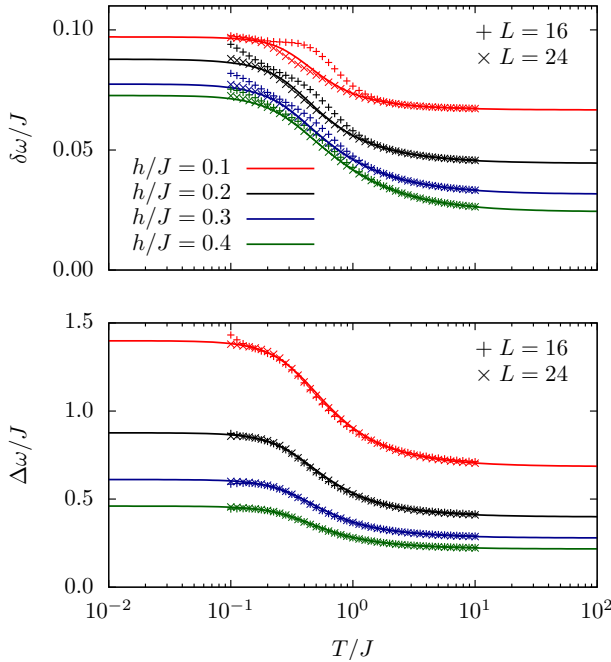


FIG. 2. Resonance shift  $\delta\omega/J$  and line width  $\Delta\omega/J$  in the critical regime at  $\delta = -0.1$  as function of the temperature. Crosses from fully numerical calculation for finite chain Hamiltonians of 16 and 24 sites.

shift  $\delta\omega$  of the average of the absorbed intensity should agree with the shift of its maximum, which is the common measure

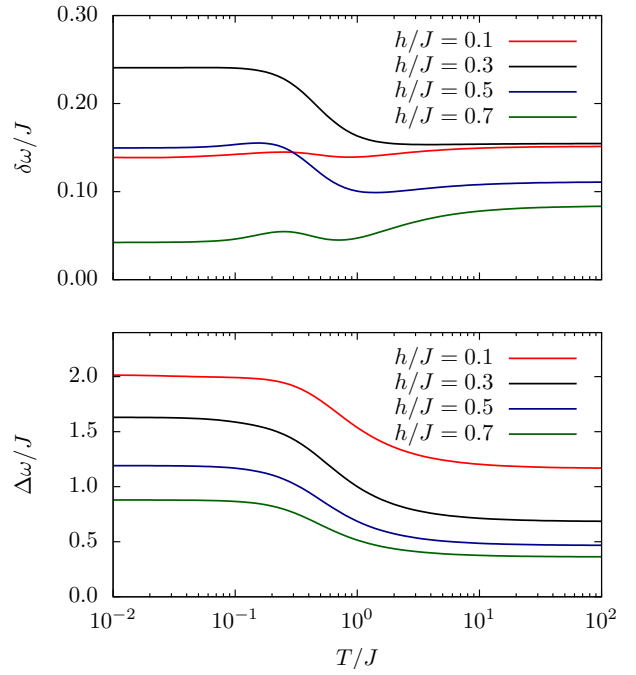


FIG. 3. Resonance shift  $\delta\omega/J$  and line width  $\Delta\omega/J$  in the massive regime at  $\delta = 0.25$  as function of the temperature.

in experiments.

For other values of the anisotropy parameters the resonance shift and the line width in the critical regime for,  $-1 \leq \delta < 0$ , show a qualitatively similar behavior as in Figs. 1 and 2. Both,  $\delta\omega$  and  $\Delta\omega$ , increase with decreasing temperature at fixed magnetic field. Note that in the massive regime, exemplified with Fig. 3, the resonance shift may behave non-monotonically as a function of temperature.

## B. Frequency-dependent moments

In order to obtain the resonance shift and the line width as defined in the previous section experimentally one would have to measure the microwave absorption at fixed Zeeman field  $h$  for various values of the frequency  $\omega$  and then calculate the required averages as integrals over  $\omega$ . In current ESR experiments different data sets are recorded. The microwave frequency  $\omega$  is kept fixed and the absorbed intensity  $I(\omega, h) = \omega\chi''_{+-}(\omega, h)/2$  is determined as a function of  $h$ . This intensity function can be normalized by dividing by its  $h$ -integral, and the corresponding frequency-depending moments define the resonance shift and line width in ‘ $h$ -direction’. Away from the isotropic point ( $\delta = 0$ ), where  $\chi''_{+-}(\omega, h)$  is symmetric and the absorption line is extremely narrow, these may be rather unrelated to their field-dependent counterparts of the previous section.

In analogy with (5) we define the frequency-dependent moments

$$M_n(T, \omega) = J^{-n} \int_{-\infty}^{\infty} \frac{dh}{2\pi} (h - \omega)^n \chi''_{+-}(\omega, h). \quad (12)$$

These can be expressed in terms of the  $m_n$  and their derivatives. Denoting the  $k$ th derivative with respect to the second argument by a superscript ( $k$ ) we obtain the representation

$$M_n(T, \omega) = (-1)^n \sum_{k=0}^{\infty} \frac{(-J)^k}{k!} m_{k+n}^{(k)}(T, \omega), \quad (13)$$

for the frequency-dependent moments. This representation involves static correlation functions for arbitrarily large distances. For this reason the  $M_n$  cannot be calculated by our exact method above. Yet, in certain cases finitely many terms of the series are sufficient for a good approximation.

We first of all express the resonance shift  $\delta h = \langle h \rangle - \omega$  and the mean square deviation from the center of the absorption peak  $\Delta h^2 = \langle h^2 \rangle - \langle h \rangle^2$  in terms of the  $M_n$ ,

$$\frac{\delta h}{J} = \frac{M_1}{M_0}, \quad \frac{\Delta h^2}{J^2} = \frac{M_2}{M_0} - \frac{M_1^2}{M_0^2}. \quad (14)$$

There are at least two cases, where these formulae simplify and finitely many of the  $m_n$  are enough to determine a systematic approximation to  $\delta h$  and  $\Delta h$ .

The equation for the resonance shift simplifies for small anisotropy,  $|\delta| \ll 1$ . Since  $M_0 = m_0 + \mathcal{O}(\delta)$ ,  $M_1 = -m_1 + \mathcal{O}(\delta^2)$  and, generically,  $m_1$  itself is of order  $\delta$  (see (10), (13)) we obtain to linear order in  $\delta$

$$\frac{\delta h}{J} = -\frac{m_1}{m_0}. \quad (15)$$

In previous work<sup>2,8</sup> the same equation was obtained by a more intuitive reasoning. It leads to results which compare rather well with experiments.<sup>8</sup> However, some care is necessary with the interpretation of (15). Since  $m_1/\delta$  vanishes at  $\delta = h = 0$ , it follows that  $m_1 = \delta(a h + b \delta + \dots)$  with some coefficients  $a, b$ , whence  $h/J$  must be large compared to  $\delta$  for (15) to be applicable.

Recall that the higher moments  $m_n$ ,  $n \geq 2$ , are of order  $\delta^2$ . Hence, for the line width there is no simplification for small anisotropy, like in (15). But there is another measurable quantity which does allow for a systematic small- $\delta$  expansion to first order, namely the integrated intensity  $\pi \omega M_0$ , since

$$M_0 = m_0 - J m_1'. \quad (16)$$

For the resonance shift it follows to linear order in  $\delta$  from (6) and (15) that  $\delta h(T, \omega) = -\delta \omega(T, h)|_{h=\omega}$ . For the line width there is no such simple relation between  $\Delta \omega$  and  $\Delta h$ , not even for small  $\delta$ .

The representation (13) is a series in ascending powers of  $J/T$  (with still temperature-dependent coefficients). This can be used to evaluate (14) asymptotically for high temperatures. It turns out that the leading terms in the  $J/T$  expansion of  $m_1$  and  $J m_1'$  cancel each other ( $\delta h \sim \frac{h}{2T} \delta \rightarrow 0$  in the high-temperature limit  $T \gg J$ ) and

$$\frac{\Delta h}{J} = \frac{|\delta|}{\sqrt{2}} \left( 1 + \frac{(1+\delta)J}{4T} - \frac{(6\delta^2 + 10\delta + 9)J^2 + 4\omega^2}{32T^2} + \dots \right), \quad (17)$$

where  $\omega$  is the microwave frequency. This formula provides a simple means to directly measure the anisotropy parameter  $\delta$ . For  $T \rightarrow \infty$  it turns into Eq. (10) of Ref. 9 upon a proper identification of parameters.

In this case as well the momentum-based line width  $\Delta h$  is initially slightly increasing from its infinite-temperature limit  $|\delta|/\sqrt{2}$  when the temperature is reduced. But our numerical data (see crosses in Fig. 4) and the second order term of the high-temperature expansion show that  $\Delta h$  behaves non-monotonically and decreases again for temperatures lower than  $J$ . For small temperatures it seems to approach zero linearly. The latter type of behavior is in accordance with field theoretical predictions<sup>5</sup> and experimental results.<sup>3,4</sup> We would like to stress, however, that there is no contradiction between the broadening shown by the upper curve in the first panel of Fig. 4 and the narrowing shown by the lower curve. In fact, both curves were obtained from the same numerical data set for the dynamical susceptibility. The upper curve was calculated with (7), whereas the lower curve was calculated by means of (14). What is important is that the upper curve can be compared with our exact results (solid line in the upper panel). The good agreement of the crosses with the exact curve creates confidence in our numerical data. It shows that they are reliable when used in integrations. This is a non-trivial statement, since our numerical data happen to be noisy and finite-size affected at low temperatures (see Sec. V E).

We would like to point out that the resonance shift  $\delta \omega/J$  or  $\delta h/J$  and the line width  $\Delta \omega/J$  or  $\Delta h/J$  defined in terms of moments show a simple scaling behavior. They depend on the exchange interaction only through the ratios  $T/J$  and  $h/J$ . In this sense the curves in Figs. 1-4 are universal.

The method of moments is not only useful for the integrable Heisenberg-Ising chain. It may be applied to non-integrable spin chains and to two- and three-dimensional models as well. The field-dependent moments and the corresponding shifts and widths may be accurately calculated by approximate methods, since they are determined by static short-range correlation functions. For a discussion of the numerical calculation of the moments in one dimension see below. In any case, the frequency-dependent moments are harder to obtain, since they require the calculation of an infinite number of static correlation functions.

### C. Integrated intensity

An important quantity in experiments of electron spin resonance is the integrated intensity.<sup>21</sup> As in the definition of the moments we may either integrate over the frequency or over the magnetic field. For fixed magnetic field  $h$  our definition (5) of the moments  $m_0$  and  $m_1$  implies that

$$\int_{-\infty}^{\infty} d\omega \frac{\omega}{2} \chi''_{+-}(\omega, h) = \pi (J m_1 + h m_0). \quad (18)$$

As explained in the previous section, in usual ESR experiments the absorbed intensity is measured as function of  $h$  for fixed microwave frequency  $\omega$ . By definition the corresponding

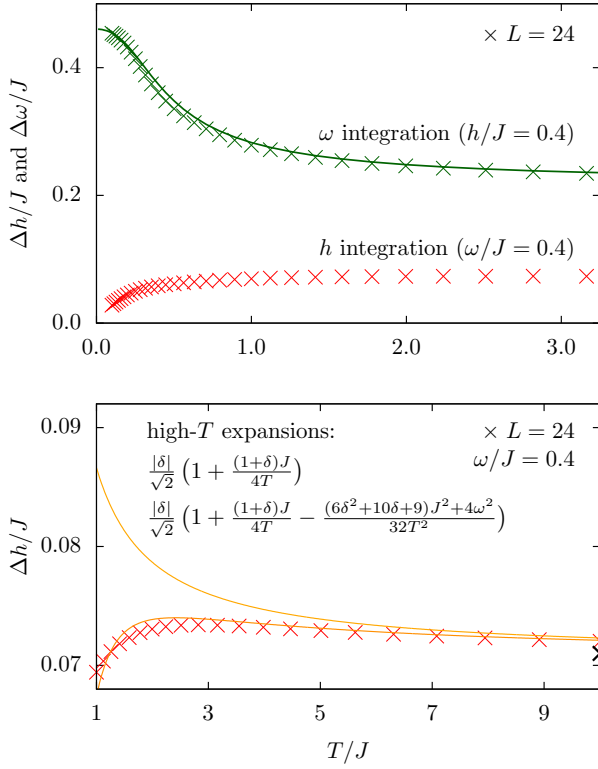


FIG. 4. Line widths  $\Delta\omega/J$  (green) and  $\Delta h/J$  (red) in the critical regime at  $\delta = -0.1$  as functions of the temperature. Data from a fully numerical calculation for a finite chain Hamiltonian of 24 sites. The black cross in the lower panel marks the infinite-temperature limit  $|\delta|/\sqrt{2}$ . The solid orange lines are high-temperature expansions of  $\Delta h/J$  according to (17) up to first and second order in  $J/T$ .

integrated intensity is

$$I_{+-}^{(\text{int})}(\omega) = \int_{-\infty}^{\infty} dh \frac{\omega}{2} \chi''_{+-}(\omega, h) = \pi\omega M_0(T, \omega). \quad (19)$$

In the paramagnetic regime, where  $h$  is large compared to  $J$ , the integrated intensity is proportional to the magnetization  $m(T, \omega)$ . The high-temperature expansion of the frequency-dependent moment  $M_0$ ,

$$M_0(T, \omega) = \frac{h}{4T} + \frac{Jh}{8T^2}(\delta - 1) + \dots, \quad (20)$$

following from (13), provides another means to determine the anisotropy  $\delta$  from experimental data.

### III. EXACT LINE SHAPES

As we have seen the method of moments allows us, at least in the field-dependent case, to obtain exact characterizations of the resonance shift and the line width for arbitrary temperatures, magnetic fields and anisotropy parameters for the infinite chain. Unfortunately, it does not teach us much about the actual line shapes. Even the most elementary question, how many peaks the line comprises, remains generally unanswered.

In the remainder of this work we shall try to draw at least a qualitative picture of how the lines are shaped by considering all available limiting cases, where exact results are known, and by complementing these with numerical data. In this section we review those limiting cases where exact results are known. In the following section we describe our numerical calculations. Finally, in Sec. V, we shall consider the line shapes for  $\delta > 0$  and  $T = h = 0$  in two-spinon approximation.

#### A. Heisenberg limit

The simplest case where we know the line shape exactly is the isotropic case  $\delta = 0$ .<sup>5</sup> It may be called the Heisenberg limit of the Heisenberg-Ising chain. In this case  $H$  is still a complicated many body Hamiltonian, but  $S^+$  commutes with  $H$  and the time evolution of  $S^+$  is driven by  $S^z$  alone (see App. A). Thus,  $S^+(t) = e^{-iht} S^+$ , and

$$I(\omega, h) = \pi\delta(\omega - h)hm(T, h). \quad (21)$$

This means that there is a single sharp peak, and the absorbed intensity is proportional to the magnetic energy  $hm(T, h)$  per lattice site. This case includes the familiar paramagnetic resonance (Zeeman effect) for which the magnetization is known explicitly, namely  $m(T, h) = \frac{1}{2} \text{th}\left(\frac{h}{2T}\right)$  for  $J = 0$ . In the general case the magnetization must be calculated from solutions of linear and non-linear integral equations.<sup>22</sup> In our context we infer from (9) and (11) that  $m(T, h) = m_0 = -\frac{1}{2}\varphi(0)$ , i.e. the lowest moment  $m_0$  alone characterizes the line shape.

#### B. Ising limit

The only other limiting case in which the line shape is known for all temperatures and magnetic fields is the Ising limit.<sup>23</sup> For the Ising limit we replace the Heisenberg-Ising Hamiltonian  $H \rightarrow H/\delta$  and send  $\delta \rightarrow \infty$ . Then

$$H \rightarrow H_I = J \sum_{j=1}^L s_{j-1}^z s_j^z. \quad (22)$$

Due to (8) this implies that the moments are replaced as  $m_n \rightarrow \delta^{-n} m_n$  for  $\delta \rightarrow \infty$ .

In the Ising limit the time evolution of  $S^+$  in (2) can be calculated explicitly. As we show in App. A 6 this leads to the formula

$$\frac{1}{2\pi} \chi''_{+-}(\omega, h) = \frac{1}{2}(m_2 - m_1)\delta(\omega - h + J) + (m_0 - m_2)\delta(\omega - h) + \frac{1}{2}(m_2 + m_1)\delta(\omega - h - J) \quad (23)$$

for the dynamical susceptibility.

Using this formula we can calculate the moments  $m_n$  by means of (5) and verify its consistency. Integrating over  $\omega$  we obtain indeed  $m_0$ . The integrals for the higher moments yield

$$m_n = \begin{cases} m_1 & \text{if } n \in \mathbb{N} \text{ is odd} \\ m_2 & \text{if } n \in \mathbb{N} \text{ is even,} \end{cases} \quad (24)$$

i.e. there are no ‘new moments’ for  $n > 2$ . The three independent moments  $m_0$ ,  $m_1$  and  $m_2$  correspond to the three  $\delta$ -peaks in the dynamical susceptibility. They can be calculated by means of the  $2 \times 2$  transfer matrix<sup>24</sup> of the Ising chain. Explicit expressions are shown in App. A 6.

The Ising limit is important for us, since it is easy to interpret and since it provides a physical picture for the massive phase. The eigenstates of the Ising chain Hamiltonian are tensor products of local  $s^z$  eigenstates. We infer from the spectral representation, App. A 7, that transitions can occur only between states which differ by a single flipped spin. Thus, the following transitions in which the chain absorbs the energy  $\Delta E$  are possible:

$$\begin{aligned} \dots \uparrow \uparrow \uparrow \dots &\rightarrow \dots \uparrow \uparrow \uparrow \dots, & \Delta E &= J - h \\ \dots \downarrow \uparrow \downarrow \dots &\rightarrow \dots \downarrow \downarrow \downarrow \dots, & \Delta E &= J + h \\ \dots \uparrow \downarrow \dots &\rightarrow \dots \uparrow \downarrow \dots, & \Delta E &= h \end{aligned}$$

The first two correspond to the creation of a pair of domain walls (or spinons) in one of the Néel ground states. The third one is impossible in the ground states, whence the coefficient  $m_0 - m_2$  in front of the corresponding term in (23) must vanish at zero temperature.

At finite  $\delta > 0$  the operator  $S^-$  in the spectral representation (A35) does no longer induce transitions between eigenstates. The three  $\delta$ -peaks in (23) broaden which reflects the onset of interactions between the spinons. Still, we believe that three peaks are characteristic of the massive phase,  $\delta > 0$ , at least at not too large magnetic fields. This is in accordance with our numerical data and with previous numerical work.<sup>6,7</sup> The relative height of the three peaks is still approximately well described by the relative prefactors of the  $\delta$ -peaks in (23). At  $T = 0$  in the two-spinon approximation (see below) the central peak vanishes due to the same intuitive argument as given above.

Figure 5 shows the dynamical susceptibility (23) in the Ising limit as a function of  $h/J$ . We visualize the  $\delta$ -peaks by convolving them with a Lorentzian of the form

$$\mathcal{L}(h) = \frac{J}{\pi} \frac{\varepsilon}{h^2 + \varepsilon^2}. \quad (25)$$

While in the low-temperature limit ( $T/J = 0.1$ ) the right peak at  $h = \omega + J$  is the highest, in the intermediate-temperature regime ( $T/J = 0.5, 1.0, 5$ ) the relative height of the central peak at  $h = \omega$  increases rapidly with increasing temperatures. For even higher temperatures ( $T/J = 5, 10, 50$ ) the relative height of the left peak at  $\omega = h - J$  increases as well and reaches values comparable to those of the right peak. The relative heights of the central peak and the right peak are compatible with the numerical data for  $\delta = 1$  shown in Fig. 8 of Ref. 6. The absolute value of the height of the central peak differs approximately by a factor of 8, because the authors of Ref. 6 plot the function  $\chi''_{xx} = (\chi''_{+-} + \chi''_{-+})/4$  instead of  $J\chi''_{+-}$  and scale it with a factor of  $1 + \delta = 2$ . Concerning the location of the three peaks as well as the relative and the absolute heights of the central peak and the right peak, the curves in Fig. 8 of Ref. 6 can be qualitatively explained by the exact result (23) for the dynamical susceptibility in the Ising limit.

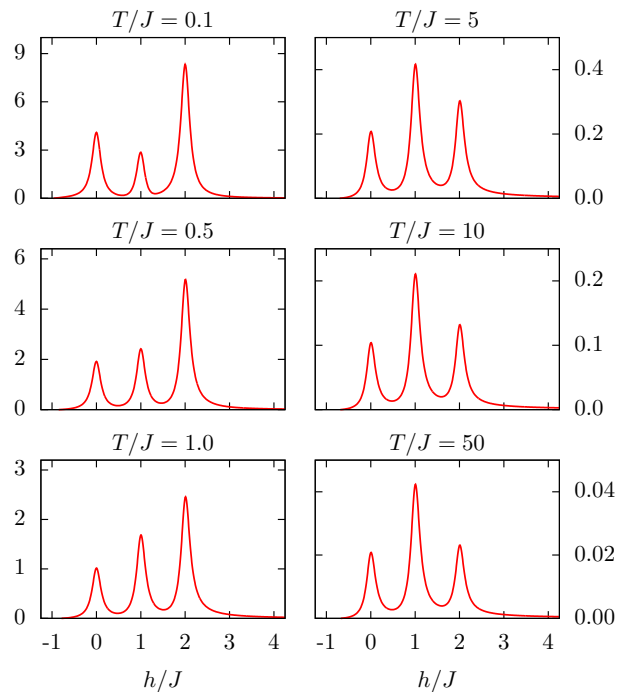


FIG. 5. Dynamical susceptibility  $J\chi''_{+-}$  from (23) as function of  $h/J$  for  $\omega = J$ . The  $\delta$ -peaks are convolved with a Lorentzian (25) with parameter  $\varepsilon = 0.12J$ .

If we use (23) and the formulae (A32) for the moments  $m_1$  and  $m_2$ , we can explicitly perform the infinite-temperature limit and obtain the function  $\phi(\omega - h)$  defined in the next section in (26) and (27). We find that its  $\delta$ -peaks are weighted by  $1/2$  for the central peak and by  $1/4$  for the two side-peaks.

### C. High-temperature limit

In the infinite-temperature limit the dynamical susceptibility  $\chi''_{+-}$  vanishes identically. This follows, for instance, from Eq. (A37). From the same equation and from the sum rule (A38) we obtain the leading high-temperature contribution to  $\chi''_{+-}$ ,

$$\chi''_{+-}(\omega, h) = \frac{\omega\pi}{2T} \phi(\omega - h) + \mathcal{O}(T^{-2}), \quad (26)$$

where

$$\phi(\omega) = \frac{2^{-L}}{\pi L} \int_{-\infty}^{\infty} dt e^{i\omega t} \text{tr}\{(e^{it\text{ad}H} S^+) S^-\}. \quad (27)$$

The function  $\phi$  is even, non-negative and normalized. Hence, it may be interpreted again as a distribution function.

The function  $\phi$  is simpler as compared to  $\chi''_{+-}$ . Still, in general, we are unable to calculate it exactly. In App. C we comment on the small- $t$  expansion of the integrand, which we have calculated up to the order  $t^3$ , and draw some conclusions. In the free Fermion case  $\delta = -1$  it is possible to calculate it to



all orders. The terms sum up to a Gaussian,<sup>25</sup> and

$$\phi(\omega) = \frac{e^{-(\omega/J)^2}}{J\sqrt{\pi}}. \quad (28)$$

From this explicit result we can calculate the field- and frequency-dependent line widths of the previous section,

$$\frac{\Delta\omega^2}{J^2} = \frac{3/2 + 2(h/J)^4}{(1 + 2(h/J)^2)^2}, \quad \frac{\Delta h}{J} = \frac{1}{\sqrt{2}}. \quad (29)$$

The second equation is in accordance with the high-temperature result (17). Our explicit example clearly shows that  $\chi''_{+-}$  is asymmetric in  $h$  and  $\omega$  and that the two line widths  $\Delta\omega$  and  $\Delta h$  are rather different quantities.

We learn from the above discussion that  $2T\chi''_{+-}(\omega, h)/\pi\omega$  is a ‘good function’. It converges to a normalized function which depends only on the difference  $\omega - h$  for  $T \rightarrow \infty$ . In the free Fermion case  $\delta = -1$  and in the isotropic case this function has a single peak at  $\omega = h$ . From our numerical data (see Fig. 6) we see that this seems to be true for all values of  $\delta$  between  $-1$  and  $0$  and even for small positive  $\delta$ . The Gaussian decay for large  $\omega$  seems to be peculiar of the free Fermion point. At all values of  $\delta$  which are larger than  $-1$  our logarithmic plots in Fig. 6 indicate an exponential decay.

When looking for a simple model for such type of line shape we found the so-called ‘normal-inverse Gaussian’,

$$\mathcal{N}(x|\alpha, \beta) = \frac{\alpha\beta e^{\alpha\beta} K_1(\alpha\sqrt{x^2 + \beta^2})}{\pi\sqrt{x^2 + \beta^2}}, \quad \alpha, \beta > 0, \quad (30)$$

where  $K_1$  is a modified Bessel function. It becomes a Gaussian in the limit  $\alpha \rightarrow \infty$ , a Lorentzian for  $\alpha \rightarrow 0$  and a  $\delta$ -function for  $\beta \rightarrow 0$ . Its moments can be easily calculated from its characteristic function

$$\tilde{\mathcal{N}}(k|\alpha, \beta) = \int_{-\infty}^{\infty} d\omega e^{ik\omega} \mathcal{N}(x|\alpha, \beta) = e^{\beta(\alpha - \sqrt{k^2 + \alpha^2})}. \quad (31)$$

For instance,

$$\langle x^2 \rangle_{\mathcal{N}} = \frac{\beta}{\alpha}, \quad \langle x^4 \rangle_{\mathcal{N}} = 3 \left( \frac{\beta^2}{\alpha^2} + \frac{\beta}{\alpha^3} \right). \quad (32)$$

This can be compared with the dimensionless moments of the distribution function  $\phi$ , which follow from (5) and (26),

$$\frac{\langle \omega^{2n} \rangle_{\phi}}{J^{2n}} = \lim_{T \rightarrow \infty} \frac{4T}{J} m_{2n-1}(T, h). \quad (33)$$

Here the right hand side can be easily calculated. If we demand that

$$\langle x^2 \rangle_{\mathcal{N}} = \frac{\langle \omega^2 \rangle_{\phi}}{J^2} = \frac{\delta^2}{2}, \quad (34a)$$

$$\langle x^4 \rangle_{\mathcal{N}} = \frac{\langle \omega^4 \rangle_{\phi}}{J^4} = \frac{\delta^2}{2} \left( \frac{3}{2} + \delta + \delta^2 \right), \quad (34b)$$

we obtain

$$\alpha = \sqrt{\frac{6}{(1+\delta)(3-\delta)}}, \quad \beta = \frac{\delta^2}{2} \sqrt{\frac{6}{(1+\delta)(3-\delta)}}. \quad (35)$$

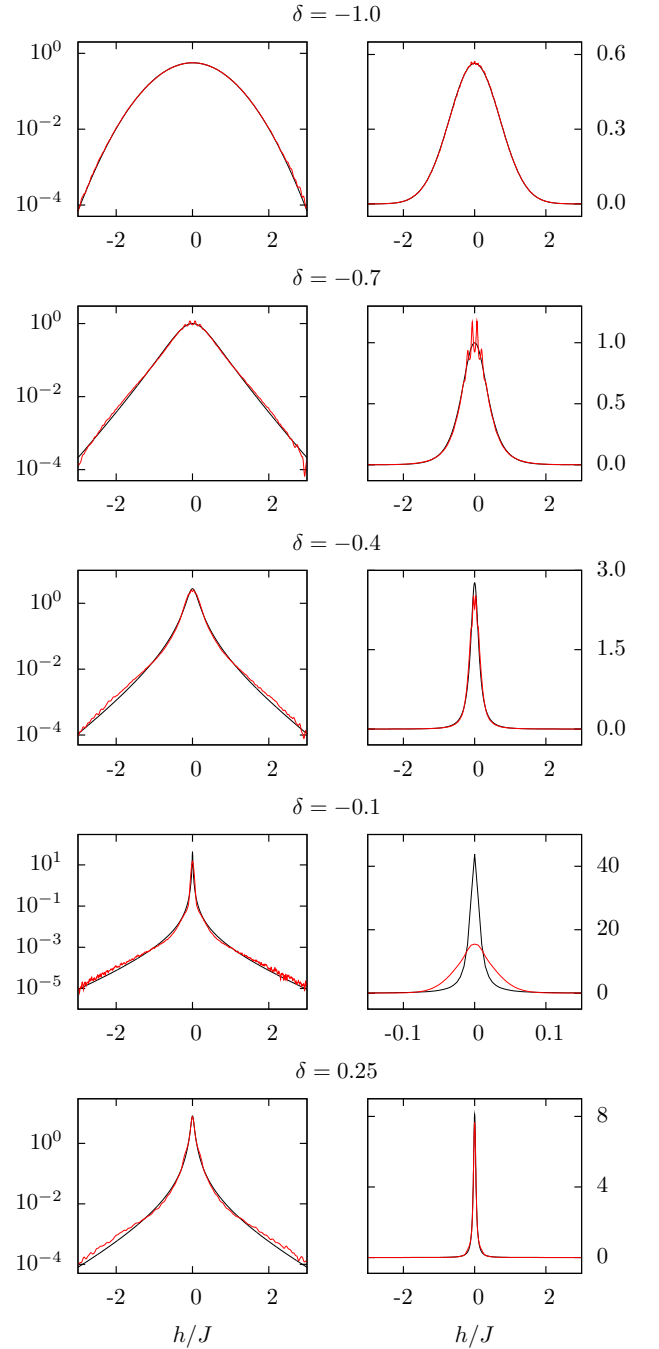


FIG. 6. Normal-inverse Gaussian (black lines) as a model for the high-temperature line shape, comparison with numerical data (red lines). Parameters of the normal-inverse Gaussian as calculated in (35). All panels show  $J\chi''_{+-}(\omega, h)$  as a function of  $h/J$ , left panels logarithmic scale, right panels linear scale. Note the different scale on the x-axis in the right panel for  $\delta = -0.1$ . In general the numerical data were obtained for  $T/J = 100$ ,  $\omega/J = 0.4$ ,  $L = 16$ , and  $M = 1024$  (see below). For  $\delta = -0.1$  the chain length was increased to  $L = 20$  and the resolution to  $M = 4096$ .

Figure 6 compares the normal-inverse Gaussian with parameters (35) with our numerical high-temperature line shapes.

For  $\delta = -1$  the model line shape is exact. This is no longer the case for  $\delta > -1$  which can be seen by comparing the sixth normalized moment of  $\phi$  with the sixth moment of  $\mathcal{N}$ . Still, we find it remarkable how well the model line shape fits our numerical data. Especially the exponential tails visible in the left panels of Fig. 6 have not been fitted to the numerical data. The good agreement comes out automatically. On the other hand, the deviation of the center of the peak in the right panel for  $\delta = -0.1$  in Fig. 6 does not seem to be due to a resolution problem of our numerical calculation. We rather attribute it to a slight mismatch of the normal inverse Gaussian at small anisotropy.

If we fix the parameters  $\alpha$  and  $\beta$  of  $\mathcal{N}(x|\alpha, \beta)$  according to (35), we see from (34a) that the width, calculated by its second moment, behaves as  $\sqrt{\langle x^2 \rangle_{\mathcal{N}}} \sim |\delta|$ . On the other hand, it is easy to calculate the peak-to-peak width of the normal-inverse Gaussian, which is the distance of its two inflection points. Setting the second derivative  $\partial_x^2 \mathcal{N}(x|\alpha, \beta)$  to zero and using the differential equation defining  $K_1$ ,

$$y^2 K_1''(y) = (y^2 + 1)K_1(y) - yK_1'(y), \quad y = \alpha\sqrt{x^2 + \beta^2}, \quad (36)$$

we see that the positive inflection point  $y_0$  is the solution of the equation

$$\frac{1}{y} + \frac{y(y^2 - (\alpha\beta)^2)}{3y^2 - 4(\alpha\beta)^2} = \partial_y \ln(K_1(y)). \quad (37)$$

In principle this algebraic equation can be solved numerically, but for our purposes the following argument leading to an estimation for the inflection point is sufficient. Since  $\partial_y \ln(K_1(y)) < -1$  for all  $y \geq 0$  and the left-hand side becomes large and positive for  $y \rightarrow 0, \infty$ , the solution  $y_0$  has to be located close to the left of the pole. Hence, we obtain

$$y_0 \lesssim \sqrt{\frac{4}{3}}\alpha\beta \quad \Rightarrow \quad x_0 \lesssim \frac{\beta}{\sqrt{3}}. \quad (38)$$

An upper limit of the peak-to-peak width is therefore given by

$$\frac{\Delta_{\text{pp}x}}{J} = 2x_0 \lesssim \delta^2 \sqrt{\frac{2}{(1+\delta)(3+\delta)}} \sim \delta^2. \quad (39)$$

Accordingly, the normal-inverse Gaussian is an example of a distribution for which the width calculated by its second moment ( $\sim |\delta|$ ) and the peak-to-peak width ( $\sim \delta^2$ ) behave asymptotically differently for small anisotropies  $\delta$  and can therefore differ strongly in value. Fitting experimental data at high temperatures to a normal-inverse Gaussian, this offers a way to determine  $\delta$  independently of the exchange integral  $J$  from the ratio of the two line widths,

$$\frac{\Delta_{\text{pp}x}}{\sqrt{\langle x^2 \rangle_{\mathcal{N}}}} \approx \frac{2|\delta|}{\sqrt{(1+\delta)(3+\delta)}}. \quad (40)$$

If we estimate the peak-to-peak width of Fig. 6 of Ref. 26 to  $\Delta_{\text{pp}h} \approx 2\text{kOe} \hat{=} 0.27K$ , we can solve (39) numerically ( $J = 22K$ ) and obtain  $\delta \approx -0.12$ . This value is compatible with the prediction of Maeda et al.<sup>8</sup> ( $\delta = -0.15$ ) obtained from a fit for

the resonance shift based on the data of Ref. 26. The authors of Ref. 27 obtain for the same material as in Ref. 26 ( $\text{LiCuVO}_4$ ) the exchange integral  $J = 30K$ . From Fig. 4 therein we can read off  $\Delta_{\text{pp}h} = 1.5\text{kOe}$ , and obtain together with Eq. (39) the anisotropy  $\delta \approx -0.088$  which is compatible with the value  $J_{zz}/J \approx -2K/30K \approx -0.067$  of Ref. 27.

#### IV. NUMERICAL LINE SHAPES

The numerical approach we are using for the calculation of the dynamical susceptibility  $\chi''_{+-}(\omega, h)$ , Eq. (2), has been described in detail elsewhere.<sup>28</sup> We will therefore give only a short outline of the method and discuss a few special tricks beneficial for the present project.

Starting point of the numerics for finite chains is the spectral representation (see also App. A 7),

$$\begin{aligned} \chi''_{+-}(\omega, h) &= \frac{\pi}{LZ} \sum_{m,n} (e^{-E_n/T} - e^{-E_m/T}) \\ &\quad \times |\langle m|S^-|n \rangle|^2 \delta(\omega - E_m + E_n) \\ &= \frac{\pi}{LZ} \int_{-\infty}^{\infty} dy s(y + \omega, y) (e^{-y/T} - e^{-(y+\omega)/T}), \end{aligned} \quad (41)$$

which can be written as an integral over thermal weighting factors and the temperature-independent function

$$s(x, y) = \sum_{m,n} |\langle m|S^-|n \rangle|^2 \delta(x - E_m) \delta(y - E_n). \quad (42)$$

At first sight the calculation of this function seems to require knowledge of all eigenvectors and eigenvalues of the Heisenberg-Ising Hamiltonian on a finite lattice. However, it is significantly more efficient to rescale all energies  $E \rightarrow \tilde{E} = aE + b$ , such that  $\tilde{E} \in [-1, 1]$ , and to expand  $s(\tilde{x}, \tilde{y})$  in terms of Chebyshev polynomials of the first kind  $T_i$ ,

$$s(\tilde{x}, \tilde{y}) = \sum_{i,j=0}^{M-1} \frac{\mu_{ij} g_i g_j (2 - \delta_{i0})(2 - \delta_{j0}) T_i(\tilde{x}) T_j(\tilde{y})}{\pi^2 \sqrt{(1 - \tilde{x}^2)(1 - \tilde{y}^2)}}. \quad (43)$$

The problem then reduces to the calculation of the expansion coefficients  $\mu_{ij}$  which are given by traces,

$$\mu_{ij} = \iint_{-1}^1 dx dy s(x, y) T_i(x) T_j(y) = \text{tr}[S^+ T_i(\tilde{H}) S^- T_j(\tilde{H})]. \quad (44)$$

Instead of summing over the whole Hilbert space, these traces are well approximated by averages over a few random states. The action of  $T_k(\tilde{H})$  on an arbitrary state can be quickly evaluated with the recursion relations of the Chebyshev polynomials. Taking into account symmetries of the Hamiltonian ( $S^z$ -conservation and translation), it is thus feasible to calculate the  $\mu_{ij}$  for systems of up to  $L = 32$  lattice sites and expansion orders up to  $M = 4096$  on average hardware.

Once we have a complete set of expansion coefficients  $\mu_{ij}$  for a given lattice size  $L$ , anisotropy  $\delta$  and all  $S^z$  sectors, we obtain  $s(x, y)$  from Eq. (43) using fast Fourier methods. In Eq. (43), the damping factors  $g_k$  cure the Gibbs oscillations

inherent to truncated Chebyshev (and Fourier) expansions, and ensure good convergence properties (see Ref. 28 for details). Given  $s(x, y)$  we can calculate  $\chi''_{+-}(\omega, h)$  for all temperatures  $T$ , frequencies  $\omega$  and magnetic fields  $h$  via straightforward numerical integration. Changing any of these three parameters does *not* require a new Chebyshev expansion, which is the most time-consuming part of the simulations.

A little more care is required for low temperatures. Here the Boltzmann factors put most of the weight on very few states at the lower edge of the spectrum. The sums in Eq. (41) should then be split up into contributions from these low-energy states and from the rest of the spectrum, and the low-energy eigenstates should be calculated exactly with Lanczos recursion.<sup>29</sup> For the data in Figs. 1 and 2 we separated two states per  $S^z$  and momentum sector from the rest of the spectrum. This procedure does not increase the overall computation time, but the book keeping is slightly more elaborate.

Another trick improves the precision of the numeric estimates of the moments  $m_n(T, h)$  and  $M_n(T, \omega)$  of  $\chi''_{+-}(\omega, h)$ , Eqs. (5) and (12), and of the resonance shifts and line widths. Since the expansion coefficients  $\mu_{ij}$  are based on averages over random vectors, they are subject to a low level of noise which is carried over to  $\chi''_{+-}(\omega, h)$ . Even though the error is hardly visible in  $\chi''_{+-}(\omega, h)$  itself, it is amplified when  $\chi''_{+-}(\omega, h)$  is multiplied by powers of  $(\omega - h)$  in the course of the moment integration. Large values of  $(\omega - h)$  taken to the power 2 or 3 then induce noticeable errors in  $m_n(T, h)$  or  $M_n(T, \omega)$ . This can be avoided by doing the multiplication with  $(\omega - h)$  in the space of Chebyshev moments. Consider a one-dimensional Chebyshev expansion of a function  $f: [-1, 1] \rightarrow \mathbb{R}$ , where the expansion coefficients are given by

$$\mu_i = \int_{-1}^1 dx f(x) T_i(x). \quad (45)$$

Then, the expansion coefficients of  $xf(x)$  are

$$\begin{aligned} \tilde{\mu}_i &= \int_{-1}^1 dx xf(x) T_i(x) = \int_{-1}^1 dx f(x) T_1(x) T_i(x) \\ &= \frac{1}{2} \int_{-1}^1 dx f(x) (T_{i+1}(x) + T_{i-1}(x)) = \frac{1}{2} (\mu_{i+1} + \mu_{i-1}). \end{aligned} \quad (46)$$

Hence, multiplication of the expanded function with the independent variable corresponds to taking a kind of mean value in the space of expansion coefficients. The application of this procedure to the two-dimensional expansion required for  $(\omega - h)^n \chi''_{+-}(\omega, h)$  leads to a cancellation of noise and to much better estimates of the moments  $m_n(T, h)$ ,  $M_n(T, \omega)$ , and of the resonance shifts and widths.

## V. TWO-SPINON LINE SHAPES

Spectral representations such as (A35), (A36) have been used in the past as a starting point for the approximate calculation of dynamical correlation functions. For the ground state case, Eq. (A36), approximate calculations can be built upon the partial summation of matrix elements of local operators between the ground state and excited states, so-called

form factors, since these are sometimes known exactly. Such type of procedure is efficient if sub-classes of form factors can be identified which contribute dominantly to the considered correlation function.

For  $-1 < \Delta := 1 + \delta \leq 1$  the Heisenberg-Ising chain is at a critical point in the ground state. In this case all form factors vanish algebraically in the thermodynamic limit.<sup>30–32</sup> Thus, the summation of form factors and the thermodynamic limit do not commute. In this case good results for the dynamic structure factor were obtained from a summation of form factors for finite chains,<sup>33–36</sup> which requires a considerable amount of numerical calculation, though. More recently, an exact summation of the leading contribution to the large distance asymptotics of two-point functions was obtained in Ref. 37.

In the massive phase at  $\Delta > 1$  the situation is mathematically less involved. Certain classes of multi-spinon form factors stay finite in the thermodynamic limit.<sup>11</sup> In calculations of the dynamic structure factor,<sup>13</sup> it turned out that the two-spinon contribution is always dominant at  $T = h = 0$ . Here we use the results of Refs. 12–14 to discuss the two-spinon contribution to the dynamical susceptibility for  $\Delta > 1$ . As we shall see, the dynamical susceptibility is dominated by the two-spinon states only if  $\Delta$  is large enough. For  $\Delta > 3/2$  the two-spinon contribution  $I^{(2)}(\omega)$  to the absorbed intensity amounts to the main part of the total intensity  $I(\omega, h = 0)$ , but it is marginal in the isotropic limit  $\Delta \rightarrow 1$ . In the Ising limit  $\Delta \rightarrow \infty$  both intensities are identical,  $I^{(2)}(\omega) = I(\omega, h = 0)$ , and the result of Sec. III B is reproduced.

A comparison of the two-spinon line shapes with numerical line shapes calculated for finite chains shows the high quality of our numerical data.

### A. Line shape

The dynamical susceptibility  $\chi''_{+-}$  decomposes into two terms, one for positive and the other one for negative frequencies. In order to calculate these terms separately we define the function

$$\chi(\omega) = \frac{1}{2L} \int_{-\infty}^{\infty} dt e^{i\omega t} \langle S^+(t) S^- \rangle_T. \quad (47)$$

Using the invariance of the Hamiltonian (1) under spin flip we obtain

$$\chi''_{+-}(\omega, h = 0) = \chi(\omega) - \chi(-\omega), \quad (48)$$

where  $\chi(\omega)$  vanishes for  $\omega < 0$  and is non-negative for  $\omega \geq 0$ .

The space of excited states decomposes into scattering states of an even number of  $2n$  spinons.<sup>38</sup> The precise mathematical structure of the space of states of the infinite XXZ chain in the massive phase was identified in Refs. 11 and 39. In order to utilize the results of Ref. 11 we have to adapt our conventions. The Hamiltonian

$$H_{JM} = -J \sum_{j=-\infty}^{\infty} (s_{j-1}^x s_j^x + s_{j-1}^y s_j^y - \Delta s_{j-1}^z s_j^z) \quad (49)$$

used in Ref. 11 is related to our Hamiltonian (1) by a unitary transformation  $s_j^{x,y} \mapsto (-)^j s_j^{x,y}$  and  $s_j^z \mapsto s_j^z$ . Under this transformation the dynamical susceptibility turns into

$$\chi(\omega) = \frac{1}{4} \sum_{k=-\infty}^{\infty} \int_{-\infty}^{\infty} dt e^{i\omega t} {}_j\langle 0 | (-)^k s_k^+(t) s_0^- | 0 \rangle_j, \quad (50)$$

where the time evolution in  $s_k^+(t)$  has to be evaluated by means of the Hamiltonian  $H_{JM}$  instead of  $H$ , and where the states  $|0\rangle_{0,1}$  are the two degenerate ground states of  $H_{JM}$ . Here we have used  $S^\pm = \sum_k s_k^\pm$ , the invariance of the Hamiltonian under translations as well as the unitary transformation defined above.

Now we insert the resolution of the identity into multi-spinon states,<sup>11</sup>

$$id_{\mathcal{F}} = \sum_{j=0,1} \sum_{n \geq 0} \sum_{\varepsilon_n, \dots, \varepsilon_1} \frac{1}{n!} \oint \frac{d\xi_n}{2\pi i \xi_n} \dots \oint \frac{d\xi_1}{2\pi i \xi_1} \times |\xi_n \dots \xi_1\rangle_{\varepsilon_n \dots \varepsilon_1, j, j, \varepsilon_1 \dots \varepsilon_n} \langle \xi_1 \dots \xi_n |, \quad (51)$$

in between the spin operators in (50) and consider only the term with  $n = 2$  which is the two-spinon contribution. The subindices  $j$  refer to the two ground-state sectors and the  $\varepsilon_\ell$  are spin indices labeling the scattering states of even numbers of spinons. In this language the two-spinon contribution is

$$\chi^{(2)}(\omega) = \frac{1}{8} \sum_{\substack{j, j'=0,1 \\ \varepsilon_1, \varepsilon_2=\pm}} \sum_k \int_{-\infty}^{+\infty} dt e^{i\omega t} \oint \prod_{i=1}^2 \frac{d\xi_i}{2\pi i \xi_i} {}_j\langle 0 | (-)^k s_k^+(t) | \xi_2, \xi_1 \rangle_{\varepsilon_2 \varepsilon_1, j, j, \varepsilon_1 \varepsilon_2} \langle \xi_1, \xi_2 | s_0^- | 0 \rangle_{j'}. \quad (52)$$

Very similar expressions were evaluated elsewhere.<sup>13,14</sup> The time evolution of  ${}_j\langle 0 | (-)^k s_k^+(t) | \xi_2, \xi_1 \rangle$  as well as the remaining form factors in (52) were obtained in Ref. 11. Inserting those results and calculating the remaining sums and integrals we end up with

$$\chi^{(2)}(\omega) = \frac{k'}{4I} \frac{\Theta(1-\hat{\omega})\Theta(\hat{\omega}-k')}{\hat{\omega}\sqrt{1-\hat{\omega}^2}\sqrt{\hat{\omega}^2-k'^2}} \frac{\vartheta_A^2(\theta)}{\vartheta_n^2(\theta)}. \quad (53a)$$

Here the factors  $\Theta$  in the numerator denote unit-step functions. The variables  $\theta$  and  $\omega$  are related as

$$\hat{\omega} = \frac{\omega}{2I} = \text{dn} \left( \frac{2K}{\pi} \theta \right), \quad 0 \leq \theta \leq \frac{\pi}{2}, \quad (53b)$$

where dn is a Jacobi elliptic function and where

$$I = \frac{JK}{\pi} \text{sh} \left( \frac{\pi K'}{K} \right). \quad (53c)$$

The anisotropy parameter  $-(1+\delta) = (q+q^{-1})/2$  is related to the nome

$$q = -\exp(-\pi K'/K), \quad (53d)$$

and thus determines the moduli  $k, k' = \sqrt{1-k^2}$  of the elliptic integrals  $K = K(k), K' = K(k')$ . The remaining theta functions

in (53) are standard and defined by

$$\vartheta_n(\theta) = \frac{\vartheta_4(\theta, p)}{\vartheta_4(0, p)}, \quad p := -q, \quad (53e)$$

$$\vartheta_A^2(\theta) = \frac{\gamma(\xi^4)\gamma(\xi^{-4})}{\gamma(q^{-2})\gamma(q^{-2})}, \quad \xi = -ie^{i\theta}, \quad (53f)$$

$$\gamma(u) = \frac{(q^4 u, q^4, q^4)(u^{-1}, q^4, q^4)}{(q^6 u, q^4, q^4)(q^2 u^{-1}, q^4, q^4)}, \quad (53g)$$

$$(x, y, z) = \prod_{m,n=0}^{\infty} (1 - xy^m z^n). \quad (53h)$$

The line shape of the function  $\chi^{(2)}$  is shown in Fig. 7 for several values of  $\Delta$ . One can observe that the broadened peak is very asymmetric for small  $\Delta$ . For increasing  $\Delta$  the peak becomes narrower and more symmetric. The Ising limit  $\Delta \rightarrow \infty$  is analyzed in the next section.

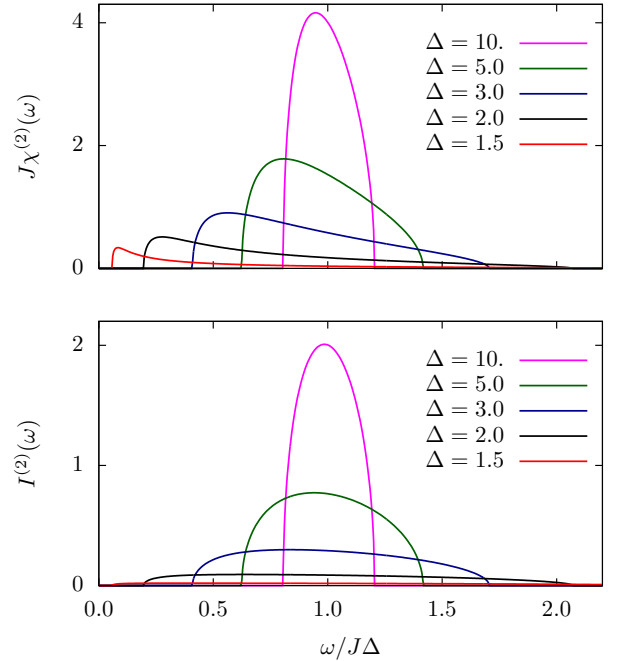


FIG. 7. Two-spinon contribution  $J\chi^{(2)}$  to the dynamical susceptibility  $J\chi_{+-}''$  and corresponding intensity  $I^{(2)}$  as functions of  $\omega/J\Delta$  for different anisotropy parameters  $\Delta > 1$  at  $T = h = 0$ .

## B. Ising limit in the two-spinon case

As the Hamiltonian (49) diverges for  $\Delta \rightarrow \infty$  we rescale all energies by the factor  $\Delta$ . Replacing, in particular,  $J$  by  $J/\Delta$  in (49), we obtain the Ising Hamiltonian (22) in the limit  $\Delta \rightarrow \infty$ .

In the expression (53) for  $\chi^{(2)}$ , the rescaling only pertains to the definition (53c) of  $I$ , where  $J$  must be replaced by  $J/\Delta$ . All other relations (53e)-(53h) and particularly (53b) remain unaffected, and the Ising limit can be easily performed. Since  $\Delta = (p+p^{-1})/2$ , we conclude that  $p \rightarrow 0$  and consequently

$k \rightarrow 0$ ,  $k' \rightarrow 1$ ,  $K \rightarrow \pi/2$  as well as  $K' \rightarrow -\frac{1}{2} \ln(p) \rightarrow \infty$ . The rescaled  $I$  becomes

$$I = \frac{JK}{\pi\Delta} \text{sh}(\pi K'/K) \rightarrow -\frac{J}{2} \frac{p-p^{-1}}{p+p^{-1}} \rightarrow \frac{J}{2}. \quad (54)$$

On the one hand the product of the two unit-step functions in the numerator of (53) ensures that  $\chi^{(2)}(\omega) = 0$  for all  $\omega \neq J$ , on the other hand we show that  $\int_{-\infty}^{\infty} d\omega \chi^{(2)}(\omega) = \pi/2$  in App. B 1. Hence,  $\chi^{(2)}$  is a  $\delta$ -function with prefactor  $\pi/2$ ,

$$\chi^{(2)}(\omega) = \frac{\pi}{2} \delta(\omega - J), \quad (55)$$

which coincides with the result (23) of Sec. III B, because  $m_0 = m_2 = 0$  for  $h = 0$  and  $m_1 \rightarrow 1/2$  for  $h = 0$  and  $T \rightarrow 0$ . For the integrated intensity we easily obtain

$$\int_{-\infty}^{\infty} d\omega \frac{\omega}{2} \chi''_{+-}(\omega) = \int_0^{\infty} d\omega \omega \chi^{(2)}(\omega) = \frac{\pi J}{2}, \quad (56)$$

which agrees with Eq. (18) of Sec. II C for  $h = 0$  and  $m_1 = 1/2$ .

### C. Heisenberg limit and integrated intensity

In the Heisenberg (or isotropic) limit  $\Delta \rightarrow 1$  we have  $p \rightarrow 1$  and consequently  $k \rightarrow 1$ ,  $k' \rightarrow 0$ ,  $K' \rightarrow \pi/2$  as well as  $K \rightarrow \infty$ . Fig. 7 shows that the function  $\chi^{(2)}$  tends to zero uniformly. This is consistent with the behavior of  $\chi''_{+-}$  in the isotropic limit, Eq. (A24), because  $m(0, T) = 0$  for all temperatures  $T$ .

In order to obtain a measure for the relative contribution of  $\chi^{(2)}$  to the full susceptibility  $\chi''_{+-}$  for all  $\Delta$ , especially for the isotropic limit  $\Delta \rightarrow 1$ , we compare the two-spinon contribution of the integrated intensity

$$I_{\text{int}}^{(2)}(\Delta) = \int_0^{\infty} d\omega \omega \chi^{(2)}(\omega) \quad (57)$$

with the total integrated intensity

$$I_{\text{int}}(\Delta) = \int_0^{\infty} d\omega \omega \chi(\omega). \quad (58)$$

We denote their ratio

$$r(\Delta) = \frac{I_{\text{int}}^{(2)}(\Delta)}{I_{\text{int}}(\Delta)}. \quad (59)$$

If we substitute  $\omega$  by  $\theta$  by means of (53b), the numerator of (59) becomes

$$I_{\text{int}}^{(2)}(\Delta) = \frac{2k'KI}{\pi} \int_0^{\pi/2} d\theta \frac{\vartheta_A^2(\theta)}{\vartheta_n^2(\theta)}. \quad (60)$$

The integral on the right hand side can be easily evaluated numerically. Furthermore, we can express the behavior of  $I_{\text{int}}^{(2)}$  in the isotropic limit analytically in terms of  $1-p = \sqrt{\Delta^2 - 1} - (\Delta - 1)$ ,

$$I_{\text{int}}^{(2)}(\Delta) \xrightarrow{\Delta \rightarrow 1} C e^{-\frac{\pi^2}{2(1-p)}} (1 + \mathcal{O}(1-p)). \quad (61)$$

The derivation of this formula and the value of the constant  $C$  are shown in App. B 2.

For the denominator of (59) we use a sum rule and obtain

$$I_{\text{int}}(\Delta) = \frac{2\pi\delta J}{\Delta} (\langle s_1^x s_2^x \rangle_0 - \langle s_1^z s_2^z \rangle_0). \quad (62)$$

Using Eqs. (28), (34), and (35) of Ref. 40 the two-point correlation functions on the right hand side can be expressed by integrals which again are easy to compute numerically. We obtain

$$\begin{aligned} \langle s_1^x s_2^x \rangle_0 - \langle s_1^z s_2^z \rangle_0 &= -\frac{1}{4} + \int_{-\infty}^{\infty} \frac{dx}{\eta \text{ch}\left(\frac{\pi x}{\eta}\right)} \\ &\times \frac{3 \sin^2 x \text{ch}^4 \frac{\eta}{2} + \cos^2 x \text{sh}^4 \frac{\eta}{2} - \frac{x}{\eta} (\text{ch}^2 \frac{\eta}{2} + \frac{1}{2}) \sin 2x \text{sh} \eta}{4(\text{sh}^2 \frac{\eta}{2} + \sin^2 x)^2}, \end{aligned} \quad (63)$$

where the parameter  $\eta$  is defined by  $\Delta = \text{ch} \eta$ . An expansion close to the isotropic point  $\eta = 0$  yields

$$I_{\text{int}}(\Delta) \sim \frac{(7 - 4 \ln 2) \pi J}{120} \eta^4. \quad (64)$$

Accordingly, the total integrated intensity  $I_{\text{int}}(\Delta)$  tends to zero for  $\Delta \rightarrow 1$ , but nowhere nearly as fast as the two-spinon contribution  $I_{\text{int}}^{(2)}(\Delta) \sim e^{-\pi^2/2(1-p)}$ . We conjecture that, close to the isotropic point  $\Delta = 1$ , all higher spinon contributions  $\chi^{(2n)}$ ,  $n \geq 2$ , are as marginal as  $\chi^{(2)}$ , but in such a way that for the full susceptibility  $\chi = \sum_{n \geq 1} \chi^{(2n)}$  still holds.

In Fig. 8 the ratio  $r$  is plotted as a function of the anisotropy  $\Delta > 1$ . For  $\Delta > 3/2$  the two-spinon contribution accounts for more than 80% of the integrated intensity, for  $\Delta > 2$  for even more than 96%. In the limit  $\Delta \rightarrow \infty$  it rapidly approaches 100%. Additionally, one can observe in the inset of Fig. 8 the over-exponential decay (61) for  $\Delta \rightarrow 1$ .

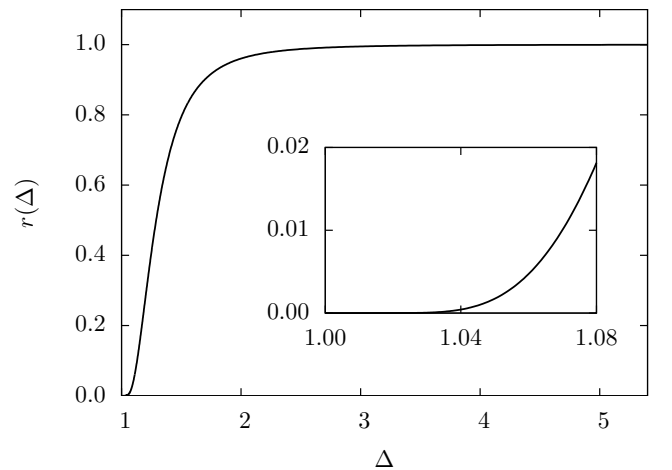


FIG. 8. Ratio  $r$  as a function of the anisotropy  $\Delta > 1$ . The inset shows the behavior of  $r$  close to the isotropic point  $\Delta = 1$ , where it decays over-exponentially.

#### D. Line width and some moments

In this section we compare the line width of the two-spinon contribution to the dynamical susceptibility with the exact line width. For this purpose we set  $T = h = 0$  in the expressions for  $\varphi$ ,  $\omega$ , and  $\omega'$  in App. D. Then, all integrals involving functions defined as solutions of integral equations vanish and  $\varphi$ ,  $\omega$ , and  $\omega'$  are determined solely by their explicit contributions. The formula for the line width simplifies to  $\Delta\omega/J = \sqrt{m_3/m_1}$  which, for  $T = h = 0$ , is then expressed in terms of explicit integrals by means of Eq. (11). Equivalently, one may use the ground-state results for short-range correlation functions of Ref. 41. Fig. 9 shows the exact line width as a function of the anisotropy for  $\Delta > -1$ .

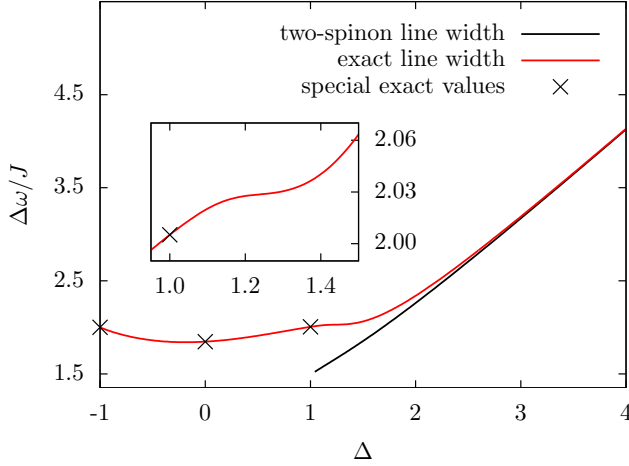


FIG. 9. Two-spinon line width  $\Delta\omega/J$  compared with the exact line width for  $T = h = 0$ . The black crosses marks the special values at  $\Delta = 1$ ,  $\Delta = 0$ , and  $\Delta = -1$ .

For the two-spinon contribution the moments  $m_1$  and  $m_3$  can be expressed by the integrals

$$m_n = \frac{(2I)^n k' K}{\pi} \int_0^{\pi/2} d\theta \, \text{dn}^{n-1} \left( \frac{2K\theta}{\pi} \right) \frac{\vartheta_A^2(\theta)}{\vartheta_n^2(\theta)}, \quad (65)$$

which can be evaluated to arbitrary precision. The two-spinon line width is shown in Fig. 9 as a function of  $\Delta > 1$ . As argued in the previous section the two-spinon contribution and the full susceptibility become identical in the Ising limit  $\Delta \rightarrow \infty$ . An expansion in  $1/\Delta$  of both line widths shows that they agree up to the order  $1/\Delta^2$ .

When  $q$  is a root of unity the moments  $m_1$  and  $m_3$  can be evaluated.<sup>41</sup> Here, we present the results for  $\Delta = 1$ ,  $\Delta = 0$ , and  $\Delta = -1$ , respectively,

$$m_1(\Delta = 1) = \frac{7 - 4 \ln 2}{15}, \quad (66a)$$

$$m_3(\Delta = 1) = -\frac{2}{5} + \frac{169}{10} \zeta(3) - \frac{18}{5} \zeta^2(3) - \frac{65}{4} \zeta(5) + \ln(2) (-4 - 10\zeta(3) + 20\zeta(5)), \quad (66b)$$

$$m_1(\Delta = 0) = \frac{2(\pi - 2)}{\pi^2}, \quad (66c)$$

$$m_3(\Delta = 0) = \frac{64 - 48\pi - 6\pi^2 + 27\pi^3}{9\pi^4}, \quad (66d)$$

$$m_1(\Delta = -1) = 1/2, \quad (66e)$$

$$m_3(\Delta = -1) = 2. \quad (66f)$$

The function  $\zeta$  is Riemann's zeta function. The numerical values of the line widths at these anisotropies are  $\Delta\omega/J \approx 2.00518$  for  $\Delta = 1$ ,  $\Delta\omega/J \approx 1.84606$  for  $\Delta = 0$ , and  $\Delta\omega/J = 2$  for  $\Delta = -1$ . Note that the exact line width as a function of  $\Delta$  is continuous and non-zero except at the isotropic points  $\Delta = 1, -1$  where it is not defined. However, the line width can be continued continuously at these points which yields the curve plotted in Fig. 9.

#### E. Comparison with numerical calculations for finite chains

We can now compare the two-spinon contribution to the dynamical susceptibility  $\chi^{(2)}$ , Eq. (53), with the full susceptibility obtained numerically by the method described in Sec. IV. For this purpose we use numerical data for  $\chi_{+-}''$  as a function of  $\omega$  for chains of lengths  $L = 24$  and  $L = 32$  at  $h = 0$  and  $\Delta = 2$ . We shall indicate the length by a subscript and briefly write  $\chi_L''$ . Based on the discussion of Sec. V C we expect that the two-spinon contribution amounts to the main part ( $\sim 96\%$ ) of the full susceptibility  $\chi_{+-}''$  in the limit  $T \rightarrow 0$ . For larger temperatures we expect deviations.

We have to comment on the limit  $T \rightarrow 0$ . For finite chains the ground state with energy  $E_0$  is non-degenerate and for  $L \bmod 4 = 0$  carries momentum  $q = 0$ . Yet, the gap  $\Delta E = E_\pi - E_0$  to the low-lying  $q = \pi$ -state is very small compared to the gaps to all other states. In the thermodynamic limit these two states degenerate and stay separated from the rest of the spectrum. Hence, for a better comparison with the two-spinon contribution, we averaged over the  $q = 0$ - and  $q = \pi$ -states in our numerical calculation shown in Fig. 10.

As one can see, at low temperature the dynamical susceptibilities  $\chi_{24}''$  and  $\chi_{32}''$  (red lines) consist of a multitude of narrow peaks. This peak-structure is due to the finiteness of the chain and the small number of eigenstates that contribute to the  $T = 0$  response. The Chebyshev expansion approach, whose resolution is inversely proportional to the expansion order  $M$ , can then distinguish all contributing matrix elements. With increasing temperature the Boltzmann factors  $\exp(-E_n/T) - \exp(-E_m/T)$ , see App. A 7, suppress fewer states, and eventually the density of the peaks becomes higher than the numeric resolution. The dynamical susceptibilities then evolve into smooth curves, as is illustrated in Fig. 11 and also by the high-temperature data in Fig. 6.

Similar behavior occurs for increasing lattice size  $L$ . Comparing the two panels of Fig. 10 one observes that the peak-structure of  $\chi_L''$  becomes tighter for larger  $L$ . Additionally, the heights of the peaks decrease. Although  $\chi_L''$  (red lines) and  $\chi^{(2)}$  (dark-blue line) do not look alike, the integrals of these two functions (orange and light-blue line) match very well. This indicates that the step function  $\int_0^\omega d\omega' \chi_L''(\omega')$  (orange line)

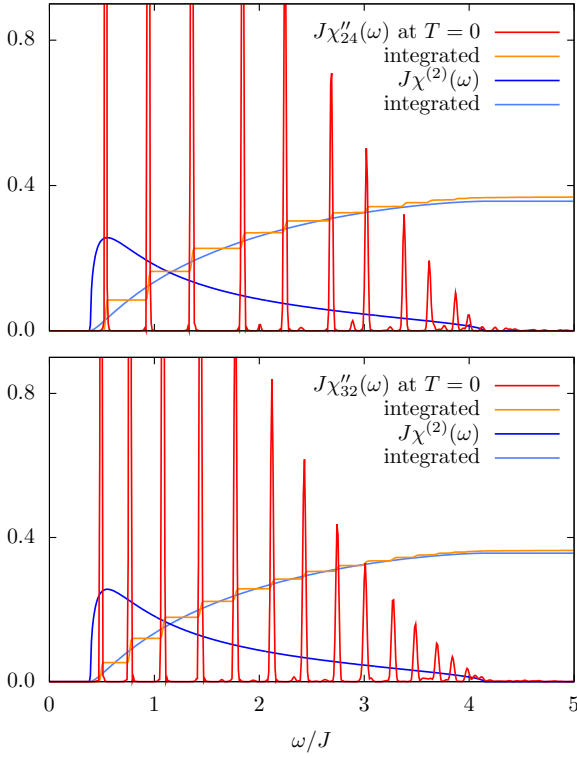


FIG. 10. Two-spinon contribution  $J\chi^{(2)}$  compared with the dynamical susceptibility  $J\chi_L''$  of finite chains as functions of  $\omega/J$  for  $\Delta = 2$  at  $T = h = 0$ .  $L = 24$  in the upper panel,  $L = 32$  in the lower panel.

converges uniformly to  $\int_0^\omega d\omega' \chi_{+-}''(\omega')$ . For the thermodynamic limit  $L \rightarrow \infty$  we expect that the peak-structure smears out and the dynamical susceptibility becomes a smooth curve akin to the two-spinon contribution  $\chi^{(2)}$ .

We conclude that at low temperature the numerically calculated line shape of the dynamical susceptibility shows strong dependence on the size of the chain and on its finite-size spectrum. By way of contrast, the moments of the dynamical susceptibility and other integrals over the whole range of frequencies seem to be well approximated by our numerical data.

## VI. CONCLUSIONS

The Heisenberg-Ising chain considered in this work is a prototypical model of a quasi one-dimensional anisotropic antiferromagnet. Its collective spinon excitations are created in pairs. Their spectrum is a scattering continuum characteristic of one-dimensional interacting systems. In microwave absorption it becomes visible in a broadening of resonances away from the isotropic point.

Within the linear response theory the absorbed intensity is basically equal to the imaginary part of the dynamical susceptibility multiplied by the absorption frequency. Although the model is exactly solvable as long as the magnetic field is directed along the axis of magnetic anisotropy, the calculation of such type of dynamical correlation functions at finite fields and

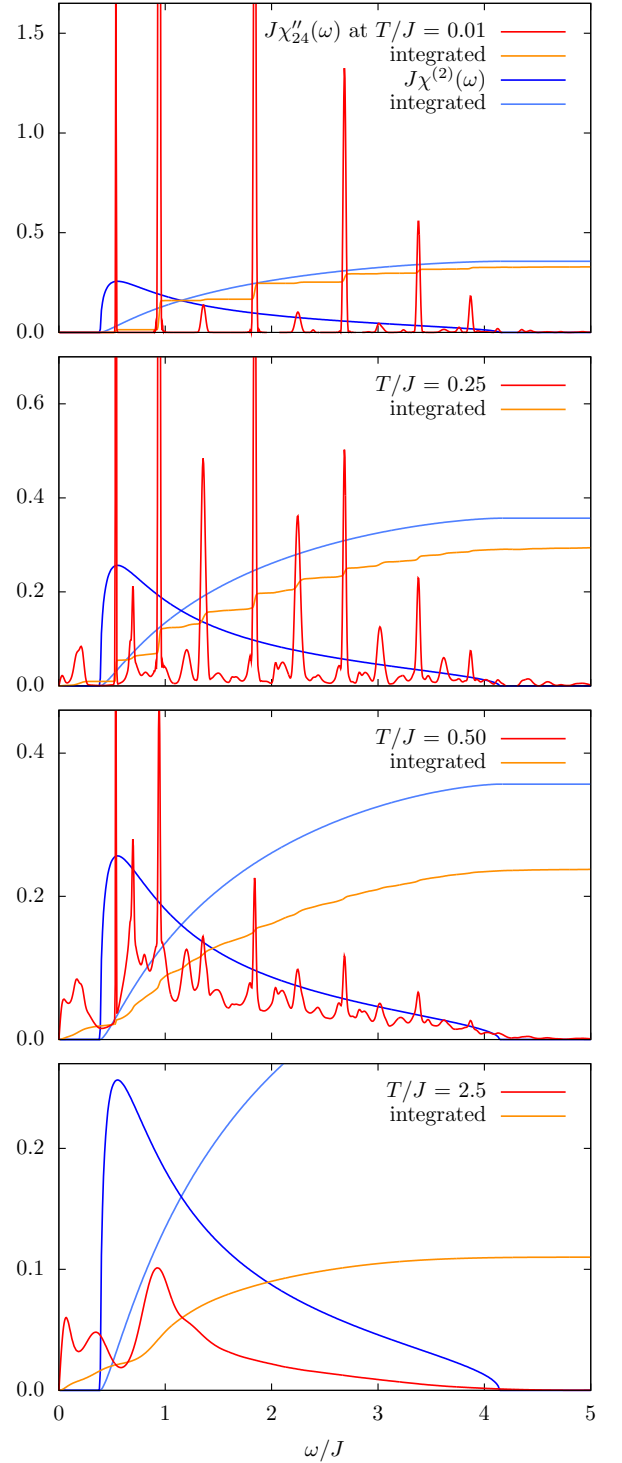


FIG. 11. Two-spinon contribution  $J\chi^{(2)}$  (dark-blue line) compared with the dynamical susceptibility  $J\chi_{24}''$  (red lines) as functions of  $\omega/J$  for  $\Delta = 2$ ,  $h = 0$  and  $L = 24$  in all panels. The temperature is increased from  $T/J = 0.01$  to  $T/J = 2.5$ . Note the different scales at the vertical axis.

temperatures is still beyond the possibilities of contemporary theoretical methods. Due to recent progress in the calculation

of static short-range correlation functions, however, it became possible to calculate certain global characteristics of the spectrum: the field-dependent moments of Sec. II that determine the average absorption frequency (the resonance shift  $\delta\omega$ ) as well as a field-dependent line width  $\Delta\omega$  at arbitrary temperatures and magnetic fields.

In this work we compared the exact data for the resonance shift  $\delta\omega$  and the line width  $\Delta\omega$  with data extracted from a numerical calculation of the dynamical susceptibility for chains of finite length. We used the exact data to improve the numerical calculation and to validate the quality of the numerical data. When looking at the numerical data for the susceptibility they appear spiky and finite-size dependent. In any case, they look rather different from the smooth curves obtained for the two-spinon contribution to the dynamical susceptibility of the infinite chain at  $T = h = 0$ , which is quasi-exact at large enough anisotropy. However, and this is an important part of the moral of our work, the picture changes if we look at integrated quantities. The integrated susceptibility for  $L = 32$  in Fig. 10 appears already rather similar to the integrated two-spinon susceptibility. When turning to moments the picture becomes even better. The numerical finite-chain data for the width  $\Delta\omega$  in Fig. 2 (where they are compared with the exact data for the infinite chain) look as if they are almost free of finite-size corrections. This gives us confidence that our data for the frequency-dependent line width  $\Delta h$ , calculated from the same numerical data set for the dynamical susceptibility, are reliable as well.

It was a big surprise for us that  $\Delta h$  shows the opposite temperature dependence in the critical phase as  $\Delta\omega$  (see Fig. 4). The line width  $\Delta\omega$  increases as the temperature decreases, but  $\Delta h$  decreases. This markedly distinct behavior can be attributed to the asymmetry of the dynamical susceptibility in  $\omega$  and  $h$ . Not only the temperature dependence of the two measures of the line width defined by the two types of moments  $m_n$  and  $M_n$  is different, but also their absolute values. We observe that  $\Delta h < \Delta\omega$ .

In general, the peak-to-peak width, usually measured in experiments<sup>3,4</sup> and decreasing with temperature, cannot be extracted from our numerical data, since they are not smooth enough at low temperatures. At high temperatures, however, where we can use the normal-inverse Gaussian as a model for  $\chi''_{+-}(\omega, h)/\omega$ , we find a peak-to-peak width  $\Delta h_{pp}$  which is again smaller,  $\Delta h_{pp} < \Delta h < \Delta\omega$ , and whose magnitude seems to be compatible with experiments.

The conclusion for theoretical attempts to extract the line width from approximations to the dynamical susceptibility is that the seemingly simple and intuitive concept of a line width is rather delicate. The peak-to-peak width, popular in the analysis of experimental data, is shape dependent and influenced by *a priori* assumptions on the line width. By contrast, our moment-based line width  $\Delta\omega$  is not based on assumptions about the shape of the spectral lines and can be calculated exactly for the Heisenberg-Ising chain. It is, moreover, universal with respect to a scaling of all quantities with the exchange interaction  $J$ . For these reasons we are curious if it will be possible in practice to obtain  $\Delta\omega$  from experimental data.

This will depend on how well background and noise can

be separated from the signal. From clean data one could even directly extract the moments  $m_1, m_2, m_3, \dots$ , defined in (5), which would mean to directly measure certain short-range correlation functions ranging over 2, 3, 4,  $\dots$  lattice sites.

As opposed to the line width the resonance shift is expected to be a more robust quantity. We expect our results for  $\delta\omega$  to compare rather directly with experimental data as long as the observed line shapes are not too much asymmetric. In the latter case the definition (6) should be taken seriously and should be used to calculate the average absorption frequency from the experimental data.

From the two-spinon result for the absorbed intensity (see Fig. 7) it can be seen that the spectral lines at low temperatures can be expected to be broad and asymmetric. In principle, the amount of asymmetry of the lines can be expressed in terms of the higher moments  $m_4, m_5$  of the dynamical susceptibility. And, in principle, these higher moments can be calculated exactly at any temperature and magnetic field, which we leave as project for future research. Another interesting project for the future may be the calculation of the  $T = 0$  dynamical susceptibility in the critical regime by means of form factors in the finite volume, in analogy with the work of Refs. 33–36 on the dynamical structure factor.

## ACKNOWLEDGMENTS

The authors would like to thank R. K. Kremer and K. Sakai for stimulating discussions and are grateful to K. Sakai for his Mathematica notebook with results for the short-range ground state correlation functions. AK and FG are indebted to Y. Maeda for a discussion in 2007 which inspired this work. MB acknowledges partial financial support by the Volkswagen Foundation.

## Appendix A: Absorption of energy in quantum spin chains

In order to keep this work self-contained we include a summary of the linear response theory of energy absorption and its application to quantum spin chains.

### 1. Time evolution of the statistical operator

We consider a quantum system with Hamiltonian  $\mathcal{H}$  possessing a discrete spectrum  $(E_n)_{n=0}^{\infty}$  and corresponding eigenstates  $\{|n\rangle\}_{n=0}^{\infty}$ . At time  $t_0$  we adiabatically switch on a time-dependent perturbation  $V(t)$ . We are interested in the time evolution of the system, assuming it was initially, at times  $t < t_0$ , in an equilibrium state described by the statistical operator

$$\rho_0 = \frac{1}{Z} \sum_{n=0}^{\infty} e^{-\frac{E_n}{T}} |n\rangle\langle n| \quad (\text{A1})$$

of the canonical ensemble. We denote the temperature by  $T$  and the canonical partition function by  $Z$ .



Let  $U(t)$  the time evolution operator of the perturbed system,

$$i\partial_t U(t) = (\mathcal{H} + V(t))U(t), \quad U(t_0) = \text{id}. \quad (\text{A2})$$

Under the influence of the perturbation the state  $|n\rangle$  evolves into  $|n, t\rangle = U(t)|n\rangle$ , and the statistical operator at time  $t$  becomes

$$\rho(t) = \frac{1}{Z} \sum_{n=0}^{\infty} e^{-\frac{E_n}{T}} |n, t\rangle \langle n, t| = U(t)\rho_0 U^{-1}(t). \quad (\text{A3})$$

We define

$$R(t) = e^{i\mathcal{H}t} (\rho(t) - \rho_0) e^{-i\mathcal{H}t}, \quad (\text{A4a})$$

$$W(t) = e^{i\mathcal{H}t} V(t) e^{-i\mathcal{H}t}. \quad (\text{A4b})$$

Then

$$\begin{aligned} i\partial_t R(t) &= i\partial_t e^{i\mathcal{H}t} U(t) \rho_0 (e^{i\mathcal{H}t} U(t))^{-1} \\ &= [W(t), e^{i\mathcal{H}t} \rho(t) e^{-i\mathcal{H}t}] = [W(t), R(t) + \rho_0]. \end{aligned} \quad (\text{A5})$$

Since  $R(t_0) = 0$  by construction, we obtain

$$R(t) = -i \int_{t_0}^t dt' [W(t'), R(t') + \rho_0]. \quad (\text{A6})$$

This Volterra equation is an appropriate starting point for a perturbation theory. Assuming that  $W(t)$  be small we conclude that

$$R(t) = -i \int_{t_0}^t dt' [W(t'), \rho_0] + \mathcal{O}(W^2), \quad (\text{A7})$$

i.e. to lowest order in  $W$

$$\rho(t) = \rho_0 - ie^{-i\mathcal{H}t} \int_{t_0}^t dt' [W(t'), \rho_0] e^{i\mathcal{H}t}. \quad (\text{A8})$$

This is the statistical operator in Born approximation. In the following  $t_0$  will be sent to  $-\infty$ .

## 2. Time evolution of expectation values

Using (A8) we can calculate the time evolution of the expectation value of an operator  $A$  due to the perturbation. Writing  $A(t) = e^{i\mathcal{H}t} A e^{-i\mathcal{H}t}$  and using the invariance of the trace under cyclic permutations we obtain

$$\begin{aligned} \delta \langle A \rangle_T &= \text{tr}\{(\rho(t) - \rho_0)A\} \\ &= -i \int_{-\infty}^t dt' \text{tr}\{[W(t'), \rho_0] e^{i\mathcal{H}t'} A e^{-i\mathcal{H}t'}\} \\ &= -i \int_{-\infty}^t dt' \langle [A(t-t'), V(t')] \rangle_T. \end{aligned} \quad (\text{A9})$$

Here  $\langle \cdot \rangle_T = \text{tr}\{\rho_0 \cdot\}$  denotes the thermal average. A typical example of a perturbation, which will be relevant for our discussion below, is a classical time-dependent field  $h^\alpha(t)$  coupling linearly to operators  $X^\alpha$ ,

$$V(t) = h^\alpha(t) X^\alpha, \quad (\text{A10})$$

$$\delta \langle A \rangle_T = -i \int_{-\infty}^t dt' \langle [A(t-t'), X^\alpha] \rangle_T h^\alpha(t'). \quad (\text{A11})$$

## 3. Absorption of energy

The absorbed energy per unit time is

$$\begin{aligned} \frac{dE}{dt} &= \frac{d}{dt} \text{tr}\{(\rho(t) - \rho_0)(\mathcal{H} + V(t))\} \\ &= -i \text{tr}\{[\mathcal{H} + V(t), \rho(t)](\mathcal{H} + V(t))\} \\ &\quad + \text{tr}\{(\rho(t) - \rho_0)\dot{V}(t)\} \\ &= \text{tr}\{(\rho(t) - \rho_0)\dot{V}(t)\} = \delta \langle \dot{V}(t) \rangle_T. \end{aligned} \quad (\text{A12})$$

Here we used (A2), (A3) in the second equation and the cyclic invariance of the trace in the third equation. Assuming that  $V(t)$  is of the form (A10) and using (A11) we obtain

$$\frac{dE}{dt} = -i \int_{-\infty}^t dt' \langle [X^\alpha(t-t'), X^\beta] \rangle_T \dot{h}^\alpha(t) h^\beta(t'). \quad (\text{A13})$$

## 4. Application to quantum spin chains

Let us now apply the above formalism to the Hamiltonian of the Heisenberg-Ising spin chain in a longitudinal static magnetic field of strength  $h$ ,

$$\mathcal{H} = J \sum_{j=1}^L (s_{j-1}^x s_j^x + s_{j-1}^y s_j^y + (1 + \delta) s_{j-1}^z s_j^z) - h S^z. \quad (\text{A14})$$

We perturb the spin chain by a circularly polarized electromagnetic wave propagating in  $z$ -direction. We assume that the wave length is large compared to the length of the spin chain and idealize this assumption by setting the wave number  $k = 0$ . Then the magnetic field component of the wave is

$$\mathbf{h}(t) = A \begin{pmatrix} \cos(\omega t) \\ -\sin(\omega t) \\ 0 \end{pmatrix}, \quad A > 0. \quad (\text{A15})$$

It couples to the total spin as

$$V(t) = h^\alpha(t) S^\alpha. \quad (\text{A16})$$

Thus,

$$\begin{aligned} \frac{dE}{dt} &= -i \int_{-\infty}^t dt' \langle [S^\alpha(t-t'), S^\beta] \rangle_T \dot{h}^\alpha(t) h^\beta(t') \\ &= \frac{A^2 \omega}{4} \int_0^\infty dt' \{ e^{i\omega(2t-t')} \langle [S^+(t'), S^+] \rangle_T \\ &\quad - e^{-i\omega(2t-t')} \langle [S^-(t'), S^-] \rangle_T + e^{i\omega t'} \langle [S^+(t'), S^-] \rangle_T \\ &\quad - e^{-i\omega t'} \langle [S^-(t'), S^+] \rangle_T \}. \end{aligned} \quad (\text{A17})$$

The ability to absorb radiation is a material property. Hence, we generally expect the absorbed energy per unit time to be proportional to the number of constituents of a physical system and to diverge in the thermodynamic limit. In order to define a quantity that truly characterizes the material and is finite in the thermodynamic limit we should therefore normalize by the

average intensity  $A^2$  of the incident wave and by the number of lattice sites  $L$ . Further averaging the normalized absorption rate over a half-period  $\pi/\omega$  of the applied field, we obtain the normalized absorbed intensity

$$\begin{aligned} I(\omega, h) &= \frac{\omega}{LA^2\pi} \int_0^{\frac{\pi}{\omega}} dt \frac{dE}{dt} \\ &= \frac{\omega}{4L} \int_{-\infty}^{\infty} dt e^{i\omega t} \langle [S^+(t), S^-] \rangle_T. \end{aligned} \quad (\text{A18})$$

Introducing the familiar (imaginary part of) the dynamical susceptibility per spin,

$$\chi''_{+-}(\omega, h) = \frac{1}{2L} \int_{-\infty}^{\infty} dt e^{i\omega t} \langle [S^+(t), S^-] \rangle_T, \quad (\text{A19})$$

the normalized absorbed intensity reads

$$I(\omega, h) = \frac{\omega}{2} \chi''_{+-}(\omega, h), \quad (\text{A20})$$

which is Eq. (3) of the main text.

### 5. The isotropic chain

The full dynamical susceptibility can only be calculated in certain special cases. In order to understand its behavior qualitatively we first of all consider the isotropic point  $\delta = 0$  of the Heisenberg-Ising chain. In this case

$$[\mathcal{H}, \mathbf{S}] = -h[S^z, \mathbf{S}], \quad (\text{A21})$$

and the Heisenberg equation of motion for the total spin  $\mathbf{S}$  can be solved,

$$\begin{aligned} \dot{S}^{\pm} &= i[\mathcal{H}, S^{\pm}] = -ih[S^z, S^{\pm}] = \mp ihS^{\pm}, \\ \Rightarrow S^{\pm}(t) &= e^{\mp iht} S^{\pm}, \end{aligned} \quad (\text{A22})$$

and  $S^z(t) = S^z$ . Hence, the total spin behaves as

$$\mathbf{S}(t) = \begin{pmatrix} \cos(ht) & \sin(ht) \\ -\sin(ht) & \cos(ht) \\ & & 1 \end{pmatrix} \mathbf{S}. \quad (\text{A23})$$

It rotates clockwise about the  $z$  axis.

On the other hand, inserting (A22) into (A19) we obtain

$$\begin{aligned} \chi''_{+-}(\omega, h) &= \frac{1}{2L} \int_{-\infty}^{\infty} dt e^{i(\omega-h)t} \langle [S^+, S^-] \rangle_T \\ &= 2\pi\delta(\omega-h)m(T, h). \end{aligned} \quad (\text{A24})$$

where  $m(T, h) = \langle S^z \rangle_T / L$  is the magnetization per lattice site. The corresponding normalized absorbed intensity is Eq. (21) in the main body of this article.

Comparing (A15), (A23) and (A24) we interpret the absorption of energy as a resonance between the rotating field of the incident wave and the rotating total spin of the chain, both spinning clockwise with frequency  $\omega = h$ . If we are off the isotropic point  $\delta = 0$  of the Hamiltonian (A14) we may expect that energy is transferred from the ‘coherent motion of the total spin’ to ‘other modes’, causing a damping of the spin precession and hence a shift and a broadening of the spectral line.

**Remark.** In other treatments of the same problem the incident wave was considered to be linearly polarized, leading to an absorbed intensity

$$\frac{\omega}{2} \chi''_{xx}(\omega, h) = \frac{\pi h}{4} m(T, h) (\delta(\omega-h) + \delta(\omega+h)). \quad (\text{A25})$$

This can be understood by taking into account that a linearly polarized wave can be decomposed into a superposition of two circularly polarized waves of opposite circular polarization. For this reason the two spectral lines in (A25) are, in fact, one and the same, when either the right circularly polarized wave has frequency  $\omega$  or the left circularly polarized wave has frequency  $-\omega$ .

### 6. The Ising chain

For the Hamiltonian  $H_I$  of Eq. (22) the time evolution  $e^{it \text{ad}_{H_I}} S^+$  can be calculated explicitly. One easily proves by induction that

$$\text{ad}_{H_I}^n S^+ = J^n \sum_{j=1}^L (s_{j-1}^z + s_{j+1}^z)^n s_j^+ \quad (\text{A26})$$

for all non-negative integers  $n$ . Furthermore

$$(s_{j-1}^z + s_{j+1}^z)^n = \begin{cases} s_{j-1}^z + s_{j+1}^z & \text{if } n \text{ is odd,} \\ \frac{1}{2} + 2s_{j-1}^z s_{j+1}^z & \text{if } n \text{ is even} \end{cases} \quad (\text{A27})$$

for all  $n \in \mathbb{N}$ . It follows that

$$e^{it \text{ad}_{H_I}} S^+ = S^+ - A + \frac{A+B}{2} e^{iJt} + \frac{A-B}{2} e^{-iJt}, \quad (\text{A28})$$

where

$$A = \sum_{j=1}^L (\frac{1}{2} + 2s_{j-1}^z s_{j+1}^z) s_j^+, \quad B = \sum_{j=1}^L (s_{j-1}^z + s_{j+1}^z) s_j^+. \quad (\text{A29})$$

Inserting (A28) into the definition of the dynamical susceptibility (2) in the Ising limit we obtain

$$\begin{aligned} \chi''_{+-}(\omega, h) &= \frac{\pi}{L} \left\{ \langle [S^+ - A, S^-] \rangle_T \delta(\omega-h) \right. \\ &\quad + \frac{1}{2} \langle [A+B, S^-] \rangle_T \delta(\omega-h+J) \\ &\quad \left. + \frac{1}{2} \langle [A-B, S^-] \rangle_T \delta(\omega-h-J) \right\}. \end{aligned} \quad (\text{A30})$$

The coefficients in front of the  $\delta$ -functions can be easily expressed in terms of the moments in the Ising limit,

$$\frac{1}{2L} \langle [A, S^-] \rangle_T = m_2 = \frac{1}{2} \langle s_1^z + 4s_1^z s_2^z s_3^z \rangle_T, \quad (\text{A31a})$$

$$\frac{1}{2L} \langle [B, S^-] \rangle_T = -m_1 = 2 \langle s_1^z s_2^z \rangle_T. \quad (\text{A31b})$$

For these correlation functions explicit expressions in terms of  $h$  and  $T$  can be obtained by means of the  $2 \times 2$  transfer matrix of the Ising chain,<sup>24</sup>

$$\langle s_1^z \rangle_T = \frac{\text{sh}\left(\frac{h}{2T}\right)}{2\sqrt{\text{sh}^2\left(\frac{h}{2T}\right) + e^{J/T}}}, \quad (\text{A32a})$$

$$\langle s_1^z s_n^z \rangle_T = \langle s_1^z \rangle_T^2 + \left(\frac{1}{4} - \langle s_1^z \rangle_T^2\right) f^{n-1}\left(\frac{h}{2T}, \frac{J}{T}\right), \quad (\text{A32b})$$

where

$$f(x, y) = \frac{\text{ch}(x) - \sqrt{\text{sh}^2(x) + e^y}}{\text{ch}(x) + \sqrt{\text{sh}^2(x) + e^y}} \quad (\text{A33})$$

and

$$\langle s_1^z s_2^z s_3^z \rangle_T = \langle s_1^z \rangle_T (2\langle s_1^z s_2^z \rangle_T - \langle s_1^z s_3^z \rangle_T). \quad (\text{A34})$$

Inserting (A31) into (A30) we obtain Eq. (23) of the main text.

## 7. Spectral representation of the dynamical susceptibility

The dynamical susceptibility has the spectral representation

$$\chi''_{+-}(\omega, h) = \frac{\pi}{LZ} \sum_{m,n} (e^{-\frac{E_n}{T}} - e^{-\frac{E_m}{T}}) \times |\langle m|S^-|n\rangle|^2 \delta(\omega - E_m + E_n) \quad (\text{A35})$$

following from (A19). Here the  $E_n$  are eigenvalues of  $\mathcal{H}$ , i.e. they include the dependence of the magnetic field.

Let  $\omega > 0$ . Then the only non-zero terms under the sum are those with  $E_m > E_n$  and those are positive. Hence,  $\chi''_{+-}(\omega)$  is non-negative for  $\omega > 0$ . Similarly,  $\chi''_{+-}(\omega)$  is non-positive for  $\omega < 0$ . It follows that  $I(\omega)$  is non-negative as was expected on physical grounds. The spectral representation simplifies for  $T \rightarrow 0$ ,

$$\chi''_{+-}(\omega, h) \rightarrow \frac{\pi}{L n_g} \sum_{n,g} \{ |\langle n|S^-|g\rangle|^2 \delta(\omega - E_n + E_g) - |\langle g|S^-|n\rangle|^2 \delta(\omega - E_g + E_n) \}. \quad (\text{A36})$$

Here we average over the  $n_g$  degenerate ground states  $|g\rangle$ . In general,  $\chi''_{+-}$  is non-vanishing even for vanishing magnetic field.

## 8. Alternative representation and a sum rule

From the spectral representation (A35) we infer that

$$\begin{aligned} \chi''_{+-}(\omega, h) &= \frac{\pi}{LZ} (1 - e^{-\frac{\omega}{T}}) \sum_{m,n} e^{-\frac{E_m}{T}} |\langle m|S^-|n\rangle|^2 \delta(\omega - E_m + E_n) \\ &= \frac{1}{2L} (1 - e^{-\frac{\omega}{T}}) \int_{-\infty}^{\infty} dt e^{i\omega t} \langle S^+(t)S^- \rangle_T. \quad (\text{A37}) \end{aligned}$$

This representation immediately implies the sum rule

$$\int_{-\infty}^{\infty} \frac{d\omega}{2\pi} \frac{\chi''_{+-}(\omega, h)}{1 - e^{-\frac{\omega}{T}}} = \frac{1}{2L} \langle S^+ S^- \rangle_T = \frac{1}{2} \sum_{j=0}^{L-1} \langle s_1^+ s_{j+1}^- \rangle_T. \quad (\text{A38})$$

Since the correlation functions  $\langle s_1^+ s_{j+1}^- \rangle_T$  decay exponentially in  $j$  in the thermodynamic limit, the integral on the left hand side exists for  $L \rightarrow \infty$ . If  $\chi''_{+-}(\omega, h)$  is analytic in the thermodynamic limit, it follows that the constant term in the Taylor expansion at  $\omega = 0$  must vanish. Then the intensity  $I(\omega, h) = \omega \chi''_{+-}(\omega, h)/2$  has a double zero at  $\omega = 0$ . Hence, it must have at least two maxima, one for  $\omega > 0$  and another one for  $\omega < 0$ .

## Appendix B: Technical details of the two-spinon calculations

### 1. Integrated susceptibility in the Ising limit

We calculate the integral of the susceptibility  $\chi^{(2)}$  over positive frequencies  $\omega$  in the Ising limit  $\Delta \rightarrow \infty$ , i.e.  $p \rightarrow 0$ ,

$$\int_0^{\infty} d\omega \chi^{(2)}(\omega) = \frac{k'K}{\pi} \int_0^{\pi/2} d\theta \frac{1}{\text{dn}\left(\frac{2K\theta}{\pi}\right)} \frac{\vartheta_A^2(\theta)}{\vartheta_n^2(\theta)}, \quad (\text{B1})$$

where we have inserted (53) and substituted  $\omega$  by  $\theta$  via the relation (53b). Due to  $K \rightarrow \pi/2$ ,  $k' \rightarrow 1$  we obtain  $\text{dn}(2K\theta/\pi) \rightarrow \text{dn}(\theta) \rightarrow 1$ ,  $\vartheta_n(\theta) \rightarrow 1$  for all  $\theta \in (0, \pi/2)$  and thereby

$$\int_0^{\infty} d\omega \chi^{(2)}(\omega) \rightarrow \frac{1}{2} \int_0^{\pi/2} d\theta \vartheta_A^2(\theta). \quad (\text{B2})$$

The limit  $p \rightarrow 0$  for the function  $\vartheta_A$  is more complicated. Using the definitions (53f)-(53h) of  $\vartheta_A$  and the relation

$$\begin{aligned} \ln \left( \prod_{n_1, \dots, n_m \geq 0} (1 - z p_1^{n_1} \dots p_m^{n_m}) \right) &= \\ &= - \sum_{n=1}^{\infty} \frac{1}{(1 - p_1^n) \dots (1 - p_m^n)} \frac{z^n}{n}, \quad (\text{B3}) \end{aligned}$$

we obtain

$$\frac{\gamma(z)}{\gamma(q^{-2})} = \exp \left( - \sum_{n=1}^{\infty} \frac{\text{sh}^2(n(\varepsilon - 2i\theta))}{\text{sh}(2n\varepsilon) \text{ch}(n\varepsilon)} \frac{e^{n\varepsilon}}{n} \right), \quad (\text{B4})$$

where  $z = e^{2i\theta}$  and  $\varepsilon = \pi K'/K$ , and therefore

$$\vartheta_A^2(\theta) = \exp \left( - \sum_{n=1}^{\infty} \frac{\text{ch}(2n\varepsilon) \cos(4n\theta) - 1}{\text{sh}(2n\varepsilon) \text{ch}(n\varepsilon)} \frac{e^{n\varepsilon}}{n} \right). \quad (\text{B5})$$

We now convert (B5) into the form

$$\begin{aligned} \ln(\vartheta_A(\theta)) &= \ln[2 \sin(2\theta)] + \sum_{n=1}^{\infty} \frac{1}{n} \frac{p^{2n}}{1 - p^{2n}} \sin^2(2n\theta) \\ &+ \sum_{n=1}^{\infty} \frac{1}{n} \frac{p^{2n}}{1 + p^{2n}} \cos^2(2n\theta) \\ &+ 2 \sum_{n=1}^{\infty} \frac{1}{n} \frac{p^{2n}}{(1 + p^{2n})^2} \cos^2(2n\theta) \quad (\text{B6}) \end{aligned}$$

and see that  $\vartheta_A(\theta) \xrightarrow{p \rightarrow 0} 2 \sin(2\theta)$ . We finally obtain

$$\int_0^\infty d\omega \chi^{(2)}(\omega) \xrightarrow{\Delta \rightarrow 1} 2 \int_0^{\pi/2} d\theta \sin^2(2\theta) = \frac{\pi}{2}. \quad (\text{B7})$$

## 2. Integrated intensity and Heisenberg limit

We analyze the behavior of the two-spinon contribution of the integrated intensity (60),

$$I_{\text{int}}^{(2)}(\Delta) = \frac{2k'I}{\pi} \int_0^{\pi/2} d\theta \frac{\vartheta_A^2(\theta)}{\vartheta_n^2(\theta)}, \quad (\text{B8})$$

in the isotropic limit  $\Delta \rightarrow 1$ , i.e.  $p \rightarrow 1$ . On the one hand, it is known that  $\vartheta_n(\theta) \rightarrow \text{ch}(2K/\pi\theta) \rightarrow \infty$ ,  $k' \rightarrow 0$  and  $I \rightarrow 0$ , on the other hand we have  $K \rightarrow \infty$  and  $\vartheta_A(\theta, p) \rightarrow \infty$ . In order to obtain more explicit results we define the function

$$f\left(\frac{2K}{\pi}\theta\right) = \lim_{p \rightarrow 1} I \vartheta_A^2(\theta), \quad (\text{B9})$$

which can be calculated as

$$f(x) = \frac{e^{-12\xi'(-1)}}{2^{4/3}} x \text{sh}(x) \left[ \psi\left(\frac{x}{\pi}\right) \right]^{-2ix/\pi} \times \exp\left\{ \frac{2i}{\pi} \int_0^x dx' \ln\left[ \psi\left(\frac{x'}{\pi}\right) \right] \right\}, \quad (\text{B10})$$

where  $\psi$  is defined by

$$\psi(x) = \frac{\Gamma(1-ix)\Gamma(1/2+ix)}{\Gamma(1+ix)\Gamma(1/2-ix)}. \quad (\text{B11})$$

Hence, we obtain

$$\begin{aligned} \kappa &:= \lim_{p \rightarrow 1} \left( \frac{I_{\text{int}}^{(2)}}{k'} \right) = \lim_{p \rightarrow 1} \left( \frac{2KI}{\pi} \right) \int_0^{\pi/2} d\theta \frac{\vartheta_A^2(\theta)}{\vartheta_n^2(\theta)} \\ &= \lim_{p \rightarrow 1} \int_0^K dx \frac{I \vartheta_A^2(\frac{\pi x}{2K})}{\vartheta_n^2(\frac{\pi x}{2K})} = \int_0^\infty dx \frac{f(x)}{\text{ch}^2 x} = 2,6471 \dots \end{aligned} \quad (\text{B12})$$

A straightforward calculation yields

$$\begin{aligned} \ln(k') &= 4 \ln[(p, p^2)] - 4 \ln[(-p, p^2)] \\ &\xrightarrow{p \rightarrow 1} -\frac{\pi^2}{2(1-p)} + 2 \ln 2 + \frac{\pi^2}{4} + \mathcal{O}(1-p). \end{aligned} \quad (\text{B13})$$

The asymptotic behavior of  $I_{\text{int}}^{(2)}$  therefore reads

$$I_{\text{int}}^{(2)}(\Delta) \xrightarrow{\Delta \rightarrow 1} C e^{-\frac{\pi^2}{2(1-p)}} (1 + \mathcal{O}(1-p)), \quad (\text{B14})$$

where  $C = 4e^{\pi^2/4} \kappa \approx 124,6$ .

## Appendix C: Short time expansion at infinite temperature

In the limit of infinite temperature the dynamical correlation functions reduce to traces of the considered time-dependent operators, and it is tempting to express the time evolution in terms of nested commutators, evaluate the traces, and obtain the leading terms of a Taylor series near time  $t = 0$ . For the spin-pair correlation function  $\langle s_n^z(t) s_0^z(0) \rangle$  such series have been calculated to orders as high as  $t^{30}$  already two decades ago.<sup>42</sup> Unfortunately, these series converge slowly and with the accessible number of terms precise values of the correlation functions can only be obtained for rather short times  $t \lesssim 5$ . Nevertheless, we performed such an expansion for  $\text{tr}[S^+(t)S^-]$ , which is at the core of the function  $\phi(\omega)$  defined in Eq. (27). Using the highly efficient computer algebra program FORM,<sup>43</sup> we computed the series up to the order  $t^{38}$ . The first few terms read

$$\begin{aligned} 2\text{Tr}[S^+(t)S^-] &\approx 1 - \frac{1}{4}(\Delta-1)^2 t^2 \\ &+ \frac{1}{96}(\Delta-1)^2(3-2\Delta+2\Delta^2)t^4 \\ &- \frac{1}{11520}(\Delta-1)^2(30-15\Delta+50\Delta^2-16\Delta^3+8\Delta^4)t^6 \\ &+ \dots \end{aligned} \quad (\text{C1})$$

Taking the logarithm we find

$$\begin{aligned} \ln(2\text{Tr}[S^+(t)S^-]) &\approx -\frac{1}{4}(\Delta-1)^2 t^2 + \Delta(\Delta-1)^2 \left[ \frac{4-\Delta}{2 \cdot 24!} t^4 \right. \\ &+ \frac{15-140\Delta+76\Delta^2-8\Delta^3}{24 \cdot 6!} t^6 \\ &+ \frac{56-2730\Delta+10948\Delta^2-8792\Delta^3+2256\Delta^4-136\Delta^5}{2^6 \cdot 8!} t^8 \\ &\left. + \dots \right], \end{aligned} \quad (\text{C2})$$

and we can immediately read off the two known results for  $\Delta = 0$  and  $\Delta = 1$ ,  $-t^2/4$  and 0, respectively. From the terms in the square bracket we were only able to sum the  $\Delta$ -free contributions and the terms of highest order in  $\Delta$ . The coefficients of the  $\Delta$ -free terms read 4, 15, 56, 210, 792,  $\dots$ , and correspond to  $\binom{2k}{k-1}$  with  $k = 2, 3, \dots$  leading to the Bessel function  $I_2$ . The coefficients of the terms with the highest power of  $\Delta$  for each power of  $t$  read 1, 8, 136, 3968, 176896,  $\dots$ , and constitute the expansion coefficients of  $\tan(x)^2$ ,

$$\frac{\tan(x)^2}{2} = \frac{1}{2!}x^2 + \frac{8}{4!}x^4 + \frac{136}{6!}x^6 + \frac{3968}{8!}x^8 + \dots \quad (\text{C3})$$

Summing these two sub-series of (C2), we obtain

$$\begin{aligned} \ln(2\text{Tr}[S^+(t)S^-]) &\approx 4\Delta(\Delta-1)^2 I_2(t) - (\Delta-1)^2 (\Delta/2)t^2 \\ &+ \frac{2(\Delta-1)^2 \ln[\cos(t\Delta/2)]}{\Delta^2}. \end{aligned} \quad (\text{C4})$$

This function does not have much value as an approximation of the considered infinite-temperature correlation function, but

it contains at least all known exact results,

$$\text{Tr}[S^+(t)S^-] \rightarrow \begin{cases} \frac{1}{2} \exp(-t^2/4) & \text{for } \Delta = 0, \\ \frac{1}{2} & \text{for } \Delta = 1, \\ \frac{1}{4}(1 + \cos(\tilde{t})) & \text{for } \Delta \rightarrow \infty, \tilde{t} = t\Delta \text{ finite.} \end{cases} \quad (\text{C5})$$

The last line corresponds to the Ising limit discussed in Sec. III B, and the Fourier transform of  $1 + \cos(\tilde{t})$  gives the three  $\delta$ -peaks of  $\phi$ , Eq. (27), where in the limit  $T \rightarrow \infty$  the side-bands have half the weight of the central peak.

#### Appendix D: Physical part of the static correlation functions

The functions  $\varphi$ ,  $\omega$ , and  $\omega'$  that determine all static correlation functions of the Heisenberg-Ising chain are defined in

$$\ln \mathfrak{b}(x) = -\frac{\pi h}{2(\pi - \gamma)T} - \frac{2\pi J \sin(\gamma)}{T\gamma \text{ch}(\pi x/\gamma)} + \int_{-\infty}^{\infty} \frac{dy}{2\pi} F(x-y) \ln(1 + \mathfrak{b}(y)) - \int_{-\infty}^{\infty} \frac{dy}{2\pi} F(x-y + \eta^-) \ln(1 + \bar{\mathfrak{b}}(y)), \quad (\text{D1a})$$

$$\ln \bar{\mathfrak{b}}(x) = \frac{\pi h}{2(\pi - \gamma)T} - \frac{2\pi J \sin(\gamma)}{T\gamma \text{ch}(\pi x/\gamma)} + \int_{-\infty}^{\infty} \frac{dy}{2\pi} F(x-y) \ln(1 + \bar{\mathfrak{b}}(y)) - \int_{-\infty}^{\infty} \frac{dy}{2\pi} F(x-y - \eta^-) \ln(1 + \mathfrak{b}(y)) \quad (\text{D1b})$$

with kernel

$$F(x) = \int_{-\infty}^{\infty} dk \frac{\text{sh}\left(\left(\frac{\pi}{2} - \gamma\right)k\right) e^{ikx}}{2 \text{sh}\left(\left(\pi - \gamma\right)\frac{k}{2}\right) \text{ch}\left(\frac{\gamma k}{2}\right)}. \quad (\text{D2})$$

Here we have introduced a parameter  $\gamma$  which provides yet another parameterization of the anisotropy,  $\delta = \cos(\gamma) - 1$ . Eq. (D1) is valid for  $0 \leq \gamma \leq \pi/2$  meaning that  $-1 \leq \delta < 0$ . Below we shall also use  $\eta = i\gamma$ . Note that the physical

terms of solutions of non-linear and linear integral equations. They were termed<sup>18</sup> the physical part of the problem, since the physical parameters like temperature or magnetic field enter solely through these functions. We shall provide their definition only for the massless case  $-1 \leq \delta < 0$ .<sup>15</sup> The definitions for the massive case can be found in Ref. 16.

First of all let us define a basic pair of auxiliary functions as the solution of the non-linear integral equations

parameters temperature  $T$ , magnetic field  $h$ , and coupling  $J$  enter only through the driving terms of Eqs. (D1) into our formulae.

Except for the auxiliary functions  $\mathfrak{b}$  and  $\bar{\mathfrak{b}}$  we need two more pairs of functions  $g_{\mu}^{(\pm)}$  and  $g'_{\mu}^{(\pm)}$  in order to define  $\varphi$ ,  $\omega$ , and  $\omega'$ . Both pairs satisfy linear integral equations involving  $\mathfrak{b}$  and  $\bar{\mathfrak{b}}$ ,

$$g_{\mu}^{(+)}(x) = \frac{i\pi}{\gamma} \text{sech}\left(\frac{\pi(x-\mu)}{\gamma}\right) + \int_{-\infty}^{\infty} \frac{dy}{2\pi} \frac{F(x-y)}{1 + \mathfrak{b}^{-1}(y)} g_{\mu}^{(+)}(y) - \int_{-\infty}^{\infty} \frac{dy}{2\pi} \frac{F(x-y + \eta^-)}{1 + \bar{\mathfrak{b}}^{-1}(y)} g_{\mu}^{(-)}(y), \quad (\text{D3a})$$

$$g_{\mu}^{(-)}(x) = \frac{i\pi}{\gamma} \text{sech}\left(\frac{\pi(x-\mu)}{\gamma}\right) + \int_{-\infty}^{\infty} \frac{dy}{2\pi} \frac{F(x-y)}{1 + \bar{\mathfrak{b}}^{-1}(y)} g_{\mu}^{(-)}(y) - \int_{-\infty}^{\infty} \frac{dy}{2\pi} \frac{F(x-y - \eta^-)}{1 + \mathfrak{b}^{-1}(y)} g_{\mu}^{(+)}(y) \quad (\text{D3b})$$

and

$$g'_{\mu}^{(+)}(x) = \left(\frac{i\pi}{\gamma}(x-\mu) - \frac{\pi}{2}\right) \text{sech}\left(\frac{\pi(x-\mu)}{\gamma}\right) + \gamma \int_{-\infty}^{\infty} \frac{dy}{2\pi} \frac{D(x-y)}{1 + \mathfrak{b}^{-1}(y)} g_{\mu}^{(+)}(y) - \gamma \int_{-\infty}^{\infty} \frac{dy}{2\pi} \frac{D(x-y + \eta^-)}{1 + \bar{\mathfrak{b}}^{-1}(y)} g_{\mu}^{(-)}(y) \\ + \int_{-\infty}^{\infty} \frac{dy}{2\pi} \frac{F(x-y)}{1 + \mathfrak{b}^{-1}(y)} g'_{\mu}^{(+)}(y) - \int_{-\infty}^{\infty} \frac{dy}{2\pi} \frac{F(x-y + \eta^-)}{1 + \bar{\mathfrak{b}}^{-1}(y)} g'_{\mu}^{(-)}(y), \quad (\text{D4a})$$

$$g'_{\mu}^{(-)}(x) = \left(\frac{i\pi}{\gamma}(x-\mu) + \frac{\pi}{2}\right) \text{sech}\left(\frac{\pi(x-\mu)}{\gamma}\right) + \gamma \int_{-\infty}^{\infty} \frac{dy}{2\pi} \frac{D(x-y)}{1 + \bar{\mathfrak{b}}^{-1}(y)} g_{\mu}^{(-)}(y) - \gamma \int_{-\infty}^{\infty} \frac{dy}{2\pi} \frac{D(x-y - \eta^-)}{1 + \mathfrak{b}^{-1}(y)} g_{\mu}^{(+)}(y) \\ + \int_{-\infty}^{\infty} \frac{dy}{2\pi} \frac{F(x-y)}{1 + \bar{\mathfrak{b}}^{-1}(y)} g'_{\mu}^{(-)}(y) - \int_{-\infty}^{\infty} \frac{dy}{2\pi} \frac{F(x-y - \eta^-)}{1 + \mathfrak{b}^{-1}(y)} g'_{\mu}^{(+)}(y), \quad (\text{D4b})$$

where

$$D(x) = \int_{-\infty}^{\infty} dk \frac{\sin(kx) \operatorname{sh}\left(\frac{\pi k}{2}\right) \operatorname{ch}\left(\left(\frac{\pi}{2} - \gamma\right)k\right)}{4 \operatorname{sh}^2\left(\left(\pi - \gamma\right)\frac{k}{2}\right) \operatorname{ch}^2\left(\frac{\gamma k}{2}\right)}. \quad (\text{D5})$$

The functions  $\omega(\mu_1, \mu_2)$ ,  $\omega'(\mu_1, \mu_2)$  and  $\varphi(\mu)$  that determine the explicit form of the correlation functions of the XXZ chain can be written as integrals involving  $\mathfrak{b}$ ,  $\bar{\mathfrak{b}}$ ,  $g_{\mu}^{(\pm)}$  and  $g'_{\mu}^{(\pm)}$ . The function

$$\varphi(\mu) = \int_{-\infty}^{\infty} \frac{dx}{2(\pi - \gamma)i} \left[ \frac{g_{\mu}^{(+)}(x)}{1 + \mathfrak{b}^{-1}(x)} - \frac{g_{\mu}^{(-)}(x)}{1 + \bar{\mathfrak{b}}^{-1}(x)} \right] \quad (\text{D6})$$

determines the magnetization  $m(T, h) = -\frac{1}{2}\varphi(0)$  which is the only independent one-point function of the XXZ chain. The function

$$\begin{aligned} \omega(\mu_1, \mu_2) = & -\frac{1}{2}K(\mu_1 - \mu_2) \\ & - \int_{-\infty}^{\infty} dk \frac{\operatorname{sh}\left(\left(\pi - \gamma\right)\frac{k}{2}\right) \cos(k(\mu_1 - \mu_2))}{i \operatorname{sh}\left(\frac{\pi k}{2}\right) \operatorname{ch}\left(\frac{\gamma k}{2}\right)} \\ & - \int_{-\infty}^{\infty} \frac{dx}{\gamma \operatorname{ch}\left(\frac{\pi(x - \mu_2)}{\gamma}\right)} \left[ \frac{g_{\mu_1}^{(+)}(x)}{1 + \mathfrak{b}^{-1}(x)} + \frac{g_{\mu_1}^{(-)}(x)}{1 + \bar{\mathfrak{b}}^{-1}(x)} \right] \end{aligned} \quad (\text{D7})$$

with

$$K(\mu) = \operatorname{cth}(\mu - \eta) - \operatorname{cth}(\mu + \eta) \quad (\text{D8})$$

also determines the energy per lattice site

$$\langle s_{j-1}^x s_j^x + s_{j-1}^y s_j^y + \Delta s_{j-1}^z s_j^z \rangle_T = \operatorname{sh}(\eta) \omega(0, 0) / 4 \quad (\text{D9})$$

of the XXZ chain. The function  $\omega'(\mu_1, \mu_2)$  is defined as

$$\begin{aligned} \omega'(\mu_1, \mu_2) = & \frac{\eta}{2} K^{(+)}(\mu_1 - \mu_2) + \int_{-\infty}^{\infty} dk \frac{\gamma \sin(k(\mu_1 - \mu_2))}{2i \operatorname{th}\left(\frac{\pi k}{2}\right) \operatorname{ch}^2\left(\frac{\gamma k}{2}\right)} \\ & - \int_{-\infty}^{\infty} \frac{dx}{\gamma \operatorname{ch}\left(\frac{\pi(x - \mu_2)}{\gamma}\right)} \left[ \frac{f_{\mu_1}^{(+)}(x)}{1 + \mathfrak{b}^{-1}(x)} + \frac{f_{\mu_1}^{(-)}(x)}{1 + \bar{\mathfrak{b}}^{-1}(x)} \right] \\ & + \int_{-\infty}^{\infty} \frac{dx (x - \mu_2)}{\gamma \operatorname{ch}\left(\frac{\pi(x - \mu_2)}{\gamma}\right)} \left[ \frac{g_{\mu_1}^{(+)}(x)}{1 + \mathfrak{b}^{-1}(x)} + \frac{g_{\mu_1}^{(-)}(x)}{1 + \bar{\mathfrak{b}}^{-1}(x)} \right], \end{aligned} \quad (\text{D10})$$

where

$$K^{(+)}(\mu) = \operatorname{cth}(\mu - \eta) + \operatorname{cth}(\mu + \eta), \quad (\text{D11a})$$

$$f_{\mu}^{(\pm)}(x) = g'_{\mu}^{(\pm)}(x) \mp \frac{i\gamma}{2} g_{\mu}^{(\pm)}(x). \quad (\text{D11b})$$

For the calculation of the moments in Sec. II the non-linear integral equations for  $\mathfrak{b}$  and  $\bar{\mathfrak{b}}$  as well as their linear counterparts for  $g_{\mu}^{(\pm)}$  and  $g'_{\mu}^{(\pm)}$  were solved iteratively in Fourier space utilizing the fast Fourier transformation algorithm. The derivatives of  $g_{\mu}^{(\pm)}$  and  $g'_{\mu}^{(\pm)}$  with respect to  $\mu$ , needed in the computation of the respective derivatives of  $\varphi$ ,  $\omega$ , and  $\omega'$  satisfy linear integral equations as well, which were obtained as derivatives of the equations for  $g_{\mu}^{(\pm)}$  and  $g'_{\mu}^{(\pm)}$ . Taking into account derivatives is particularly simple in Fourier space.

- 
- <sup>1</sup> R. Kubo and K. Tomita, J. Phys. Soc. Jpn., **9**, 888 (1954).
  - <sup>2</sup> K. Nagata and Y. Tazuke, J. Phys. Soc. Jpn., **32**, 337 (1972).
  - <sup>3</sup> Y. Ajiro, J. Phys. Soc. Jpn., Suppl. B, **72**, 12 (2003).
  - <sup>4</sup> H.-A. Krug von Nidda, N. Büttgen, and A. Loidl, Eur. Phys. J. Special Topics, **180**, 161 (2010).
  - <sup>5</sup> M. Oshikawa and I. Affleck, Phys. Rev. Lett., **82**, 5136 (1999); Phys. Rev. B, **65**, 134410 (2002).
  - <sup>6</sup> A. Ogasahara and S. Miyashita, J. Phys. Soc. Jpn., Suppl. B, **72**, 44 (2003).
  - <sup>7</sup> S. Miyashita, T. Yoshino, and A. Ogasahara, J. Phys. Soc. Jpn., **68**, 655 (1999); S. El Shawish, O. Cépas, and S. Miyashita, Phys. Rev. B, **81**, 224421 (2010).
  - <sup>8</sup> Y. Maeda, K. Sakai, and M. Oshikawa, Phys. Rev. Lett., **95**, 037602 (2005).
  - <sup>9</sup> J. H. van Vleck, Phys. Rev., **74**, 1168 (1948).
  - <sup>10</sup> M. Brockmann, F. Göhmann, M. Karbach, A. Klümper, and A. Weiße, Phys. Rev. Lett., **107**, 017202 (2011).
  - <sup>11</sup> M. Jimbo and T. Miwa, *Algebraic Analysis of Solvable Lattice Models* (American Mathematical Society, 1995).
  - <sup>12</sup> A. H. Bougourzi, M. Couture, and M. Kacir, Phys. Rev. B, **54**, R12669 (1996).
  - <sup>13</sup> A. H. Bougourzi, M. Karbach, and G. Müller, Phys. Rev. B, **57**, 11429 (1998).
  - <sup>14</sup> J.-S. Caux, J. Mossel, and I. P. Castillo, J. Stat. Mech.: Theor. Exp., P08006 (2008).
  - <sup>15</sup> H. Boos, J. Damerau, F. Göhmann, A. Klümper, J. Suzuki, and A. Weiße, J. Stat. Mech.: Theor. Exp., P08010 (2008).
  - <sup>16</sup> C. Trippe, F. Göhmann, and A. Klümper, Eur. Phys. J. B, **73**, 253 (2010).
  - <sup>17</sup> M. Jimbo, T. Miwa, and F. Smirnov, J. Phys. A, **42**, 304018 (2009).
  - <sup>18</sup> H. Boos and F. Göhmann, J. Phys. A, **42**, 315001 (2009).
  - <sup>19</sup> H. Boos, F. Göhmann, A. Klümper, and J. Suzuki, J. Phys. A, **40**, 10699 (2007).
  - <sup>20</sup> J. Sato, B. Aufgebauer, H. Boos, F. Göhmann, A. Klümper, M. Takahashi, and C. Trippe, Phys. Rev. Lett., **106**, 257201 (2011).
  - <sup>21</sup> J. Typek and N. Guskos, Rev. Adv. Mater. Sci., **12**, 106 (2006).
  - <sup>22</sup> A. Klümper, Z. Phys. B, **91**, 507 (1993).
  - <sup>23</sup> H. Shiba and K. Adachi, J. Phys. Soc. Jpn., **50**, 3278 (1981).
  - <sup>24</sup> R. J. Baxter, *Exactly Solved Models in Statistical Mechanics* (Academic Press, London, 1982).
  - <sup>25</sup> U. Brandt and K. Jacoby, Z. Phys. B, **25**, 181 (1976).
  - <sup>26</sup> A. N. Vasil'ev, L. A. Ponomarenko, H. Manaka, I. Yamada, M. Isobe, and Y. Ueda, Phys. Rev. B, **64**, 024419 (2001).
  - <sup>27</sup> H.-A. Krug von Nidda, L. E. Svistov, M. V. Eremin, R. M. Eremina, A. Loidl, V. Kataev, A. Validov, A. Prokofiev, and W. Aßmus, Phys. Rev. B, **65**, 134445 (2002).
  - <sup>28</sup> A. Weiße, Eur. Phys. J. B, **40**, 125 (2004); A. Weiße, G. Wellein,

- A. Alvermann, and H. Fehske, *Rev. Mod. Phys.*, **78**, 275 (2006);  
A. Weiße and H. Fehske, in *Computational Many-Particle Physics*,  
Lecture Notes in Physics, Vol. 739, edited by H. Fehske, R. Schnei-  
der, and A. Weiße (Springer, Heidelberg, 2008) pp. 545–577.
- <sup>29</sup> C. Lanczos, *J. Res. Nat. Bur. Stand.*, **45**, 255 (1950).
- <sup>30</sup> M. Arikawa, M. Karbach, G. Müller, and K. Wiele, *J. Phys. A*, **39**,  
10623 (2006).
- <sup>31</sup> N. Kitanine, K. K. Kozłowski, J. M. Maillet, N. A. Slavnov, and  
V. Terras, *J. Math. Phys.*, **50**, 095209 (2009).
- <sup>32</sup> N. Kitanine, K. K. Kozłowski, J. M. Maillet, N. A. Slavnov, and  
V. Terras, *J. Stat. Mech.: Theor. Exp.*, **1105**, P028 (2011).
- <sup>33</sup> D. Biegel, M. Karbach, and G. Müller, *Europhys. Lett.*, **59**, 882  
(2002).
- <sup>34</sup> D. Biegel, M. Karbach, and G. Müller, *J. Phys. A*, **36**, 5361 (2003).
- <sup>35</sup> J. Sato, M. Shiroishi, and M. Takahashi, *J. Phys. Soc. Jpn.*, **73**,  
3008 (2004).
- <sup>36</sup> J.-S. Caux and J. M. Maillet, *Phys. Rev. Lett.*, **95**, 077201 (2005).
- <sup>37</sup> N. Kitanine, K. K. Kozłowski, J. M. Maillet, N. A. Slavnov, and  
V. Terras, *J. Stat. Mech.: Theor. Exp.*, P12010 (2011).
- <sup>38</sup> J. D. Johnson, S. Krinsky, and B. M. McCoy, *Phys. Rev. A*, **8**,  
2526 (1973).
- <sup>39</sup> M. Jimbo, K. Miki, T. Miwa, and A. Nakayashiki, *Phys. Lett. A*,  
**168**, 256 (1992).
- <sup>40</sup> M. Takahashi, G. Kato, and M. Shiroishi, *J. Phys. Soc. Jpn.*, **73**,  
245 (2004).
- <sup>41</sup> G. Kato, M. Shiroishi, M. Takahashi, and K. Sakai, *J. Phys. A*, **37**,  
5097 (2004).
- <sup>42</sup> M. Böhm and H. Leschke, *J. Phys. A*, **25**, 1043 (1992).
- <sup>43</sup> J. A. M. Vermaseren, “New features of form,” (2000), preprint.